ELSEVIER

Chemical Geology 213 (2004) 359–383

CHEMICAL GEOLOGY
INCLUDING
ISOTOPE GEOSCIENCE

www.elsevier.com/locate/chemgeo

Chemical, biological and hydrological controls on the ^{14}C content of cold seep carbonate crusts: numerical modeling and implications for convection at cold seeps

G. Aloisi[a,*], K. Wallmann[a], R.R. Haese[b,1], J.-F. Saliège[c]

[a]*GEOMAR Research Centre, Wischhofstrasse, 1-3, D-24148 Kiel, Germany*
[b]*Department of Geochemistry, Faculty of Earth Sciences, Utrecht University, P.O. Box 80021, 3508 TA Utrecht, The Netherlands*
[c]*Laboratoire d'Océanographie Dynamique et de Climatologie, 4, Place Jussieu, 75005, Paris, France*

Received 28 October 2003; accepted 29 July 2004

Abstract

Understanding the hydrology of cold seep environments is crucial to perform accurate estimates of fluid and chemical fluxes at sedimentary wedges. Shallow convection processes may affect fluid flux estimates and could favor the destabilization of gas hydrate accumulations, increasing the sediment-ocean methane flux. Evidence for the occurrence of convection at cold seeps, however, is still limited. We use the concentration of ^{14}C ($D^{14}C$) in carbonate crusts formed at cold seeps of the eastern Mediterranean Sea as a tracer for convective recirculation of seawater-derived fluids. A numerical model is applied to investigate the controls on ^{14}C incorporation in cold seep carbonates. Our simulations show that increased amounts of CH_4 in the expelled fluids result in elevated crust $D^{14}C$, while high Ca^{2+} and HCO_3^- concentrations produce the opposite effect. Convection is the only transport process that can significantly increase crust $D^{14}C$. Advection, bioirrigation, eddy diffusion and bioturbation instead, have little effect on, or produce a decrease of, crust $D^{14}C$. In addition, the presence of old or modern carbon (MC) in host sediments prior to cementation and the ^{14}C-decay associated to the time needed to form the crust contribute in defining the $D^{14}C$ of carbonate crusts. We then use the model to reproduce the ^{14}C content of the eastern Mediterranean Sea crusts to constrain the chemical and hydrological conditions that led to their formation. Some crusts contain relatively low amounts of ^{14}C ($-945.0<D^{14}C$ ‰<-930.2) which, assuming no ageing after crust formation, can be reproduced without considering convection. Other crusts from two sites (the Amsterdam and Napoli mud volcanoes), instead, have a very high ^{14}C-content ($-899.0<D^{14}C$ ‰<-838.4) which can only be reproduced by the model if convection mixes deep fluids with seawater. Order-of-magnitude calculations using the Rayleigh criterion for convection suggest that the slow seepage (about 10 cm $year^{-1}$) of low salinity (20‰) fluids at the Amsterdam sites could trigger haline convection there. On the Napoli mud volcano, where high-density brines are expelled, density-driven

* Corresponding author. Present address: Laboratoire de Paléoenvironnements et Paléobiosphère Université Claude-Bernard, Lyon 12, rue Dubois 69622 Villeurbanne, Cedex, France. Fax: +49 431 6002930.

E-mail addresses: valoisi@geomar.de, Giovanni.Aloisi@univ-lyon1.fr (G. Aloisi), kwallmann@geomar.de (K. Wallmann), ralf.haese@ga.gov.au (R. Haese), jfs@lodyc.jussieu.fr (J.-F. Saliège).

[1] Geoscience Australia, Geoscience for Coastal Waterway Management, P.O. Box 378, Canberra, ACT 2601, Australia.

0009-2541/$ - see front matter
doi:10.1016/j.chemgeo.2004.07.008

convection cannot take place and other processes, possibly involving the rapid movement of free gas in the sediment, could be important.

Keywords: Cold seeps; Carbonate diagenesis; Carbon-14; Convection

1. Introduction

The expulsion of fluids from sedimentary wedges produces significant fluid and chemical fluxes (Carson et al., 1990; Suess et al., 1999). Quantifying the magnitude of these fluxes is important to constrain global geochemical cycles and to asses fluid budgets in subduction zones, where subduction accretion-induced dewatering controls the buildup of mechanical stress, affecting the distribution of earthquakes (Kastner et al., 1991; Sammonds et al., 1992). In the sedimentary wedge, fluids expelled through tectonically driven compaction are channeled in tectonic or sedimentary pathways of relatively high-permeability and reach the seafloor forming cold seeps. Estimates of fluxes from sedimentary wedges rely on measurements of the rate of fluid flow at individual seep sites, on estimates of seep density based on seafloor surveys and on extrapolations of these observations at the scale of the sedimentary wedge (Henry et al., 1992; Linke et al., 1994; Carson et al., 1990; Suess et al., 1998; Henry et al., 2002).

Work on the Cascadia (Carson et al., 1990) and Nankai (Le Pichon et al., 1991) accretionary wedges has shown that flux estimates obtained in this way can be up to several orders of magnitude higher than those expected from steady-state compaction of wedge sediments, calculated based on sediment porosity reduction (Carson et al., 1990; Suess et al., 1998) and thermal models (Le Pichon et al., 1991). Such a discrepancy may indicate that seepage is a short-lived, nonsteady-state process or that fluids are not derived locally, but are transported laterally into the area where the investigated seeps occur (Carson et al., 1990). Alternatively, increased outflow at cold seeps can be produced by convection of seawater into the sediments, triggered by the expulsion of low-salinity fluids (Henry et al., 1992). In situ flow measurements show that the shallow hydrology of cold seeps is more complex than previously thought and cannot be described by simple patterns of advective outflow (Tryon et al., 1999; Tryon and Brown, 2001). Fluid flow can be highly variable, both spatially and temporally; cold seeps include areas of outflow and downflow, characterized by time-dependent flow rates and episodes of flow reversal. These are likely the seafloor expression of convection systems whose extension and driving mechanisms may be varied and are poorly understood (Henry et al., 1992; O'Hara et al., 1995; Tryon et al., 2002). Convective mixing of seawater with deep fluids will have to be considered if localised flux measurements at cold seeps are used to estimate fluid and chemical fluxes at the scale of the sedimentary wedge. Cold seeps are sometimes associated to shallow gas hydrate accumulations (Suess et al., 1999; Macdonald et al., 2003; Van Dover et al., 2003). Regardless of the pressure and temperature conditions, the destabilization of gas hydrates may be promoted when methane in the surrounding pore fluids is consumed by biogeochemical processes. Convection, which introduces methane-free and sulfate-rich bottom waters sediments, has the potential to enhance methane consumption and promote gas hydrate destabilization, producing a transient increase of fluid and chemical fluxes (Tryon et al., 1999). Such a relationship between convection, hydrate destabilization and increased fluid fluxes has been proposed for a mud volcano in the Barbados accretionary wedge (Henry et al., 1996) and could represent a common process, rather than an exception, at cold seeps associated to dissociating gas hydrates.

Authigenic carbonates arguably provide the most common and long-lasting evidence of fluid expulsion and are widespread at cold seeps on modern and ancient accretionary wedges (Ritger et al., 1987; Sakai et al., 1992; Cavagna et al., 1999). They form through anaerobic methane oxidation (AMO) when upward-advecting, methane-charged fluids come in contact with seawater sulfate (Ritger et al., 1987). In this process, microorganisms consume methane and sul-

fate and produce sulfide and carbonate alkalinity (Hinrichs et al., 1999; Boetius et al., 2000; Mills et al., 2003), inducing the precipitation of carbonates, mainly aragonite and high-Mg calcite, near the seafloor (Peckmann et al., 2001; Aloisi et al., 2002). Chimney-like constructions and a variety of cemented fluid pathways, concretions and nodules occurring at variable depths in the sediment are formed through this process. More typically, however, cold seep carbonates occur as centimeter- to decimeter-thick crusts formed at very shallow depth in the sediment, where the highest AMO rates and carbonate supersaturation occur (Luff and Wallmann, 2003). Crusts of this type are exposed at the seafloor by erosion or gravitational processes and cover large portions of the seafloor in several cold seep areas worldwide (e.g. Faugères et al., 1997; Paull et al., 1992).

Modern cold seep carbonates commonly contain appreciable amounts of ^{14}C (up to 10% modern carbon; Paull et al., 1989; Lalou et al., 1992; Aharon et al., 1997; Peckmann et al., 2001). Determining their ^{14}C content, however, has not proven to be particularly useful in understanding cold seep processes, mainly because the ^{14}C dating method is not applicable in this setting. Although modern pelagic sediment (Paull et al., 1989) and young, biogenic methane (Peckmann et al., 2001) can provide some of the ^{14}C, seawater dissolved inorganic carbon (DIC) (Lalou et al., 1992; Aharon et al., 1997) is often the main, and sometimes the only, ^{14}C source in cold seep settings. Bottom water ^{14}C is incorporated in cold seep carbonates through downward molecular diffusion of ^{14}C-bearing DIC. However, if convection is active during crust formation, it should provide a supplementary source of ^{14}C leading to the formation of crusts with anomalously high ^{14}C contents, compared to crusts formed without convection.

In this study, we use ^{14}C as a tracer of chemical, biological and hydrological processes that are involved in carbonate crust formation. A numerical model that simulates the formation of carbonate crusts at cold seeps is developed to identify the factors that control their ^{14}C content. New ^{14}C data are presented from carbonate crusts formed at cold seeps of eastern Mediterranean Sea mud volcanoes. Their ^{14}C content is reproduced numerically providing some constrains on the prevailing chemical and hydrological conditions and indicating that convection was active during the formation of some of the crusts.

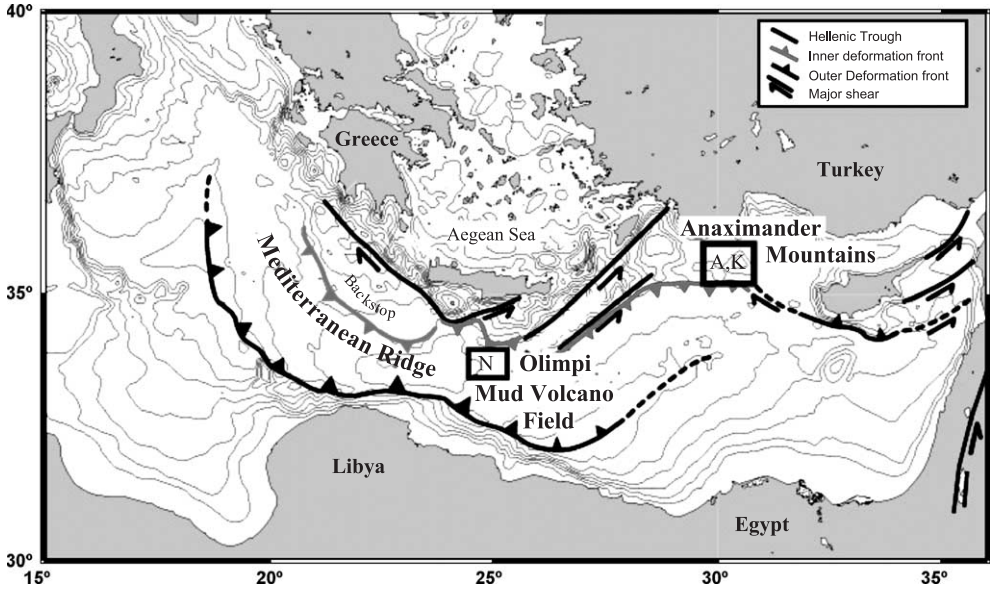

Fig. 1. Location of the Olimpi area and the Anaximander Mountains area where 20 *Nautile* submersible dives explored methane seepage areas located on mud volcanoes and associated to faults during the Medinaut cruise in 1998. The Napoli mud volcano (N) is in the Olimpi area, the Amsterdam (A) and Kazan (K) mud volcanoes are in the Anaximander Mountains area.

2. Mud volcano sites, samples and methods

Mud volcanoes are common in the eastern Mediterranean, both on the Mediterranean Ridge (Cita et al., 1996a) and in the Anaximander Mountains area (Fig. 1, Woodside et al., 1998). They form when tectonically overpressured and methane-charged sediment/fluid mixtures ('mud breccia'; Cita et al., 1981) are expelled on the seafloor. *Nautile* submersible dives explored seven of these mud volcanoes during the MEDINAUT cruise of R/V *Nadir* in 1998 showing that they are actively emitting methane-charged fluids as well as brines (MEDINAUT and MEDINETH Shipboard Scientific Parties, 2000). These sites of methane emission share sedimentological, chemical and biological features common to other cold seep areas worldwide, including methane plumes, chemosynthesis-based benthic communities and authigenic carbonate crusts pavements formed through AMO (Aloisi et al., 2002). Erosion of surface sediments and/or the post emplacement remobilization of mudflows has uncovered large portions of crust pavements resulting in crusts outcropping at the seafloor (Fig. 2a; Aloisi et al., 2000). The chemistry of fluids expelled at eastern Mediterranean cold seep sites was determined by De Lange and Brumsack (1998), Haese et al. (2003); Haese et al. (submitted for publication). The dissolved calcium, inorganic carbon (DIC) and methane concentration for the sites included in our study is shown in Table 1. Dissolved methane was found to reach equilibrium with gas hydrates (120 mM; Zatsepina and Buffet, 1997) below 1–2 m sediment depth at sites on the Kazan mud volcano.

Carbonate crusts were sampled by breaking off pieces of crust from outcropping carbonate layers during submersible dives. Most carbonate crusts included in this study belong to two types (Table 2):

(1) *Mud breccia crusts* derive from the lithification of mud breccia deposits. Those sampled from the Amsterdam mud volcano consist of millimeter-to centimeter-sized rock fragments immersed in a finer matrix/cement (Fig. 2b), a texture which strongly resembles that of ordinary, unlithified, mud breccia (Akhmanov and Woodside, 1998). Their lithification decreases with depth in the sediment and they are commonly traversed by a great number of sinuous tubular voids generally under 1 cm in diameter, most probably formerly occupied by pogonophoran tube worms (Aloisi et al., 2000). Bivalves can be attached to the upper or lower surface of the crust. Mud breccia crusts sampled from the Napoli mud volcano, instead, have a fine-grained texture reflecting the fine-grained nature of the 'mousse-like' mud breccia erupted from this mud volcano (Cita et al., 1996b).

(2) *Pelagic crusts* derive from the lithification of pelagic deposits. Two pelagic crusts were sampled from the Kazan mud volcano which is partly draped by pelagic deposits. Pelagic crusts do not show a particular internal texture other than a fine-grained carbonate cement containing the tests of calcareous planktonic organisms (Fig. 2c).

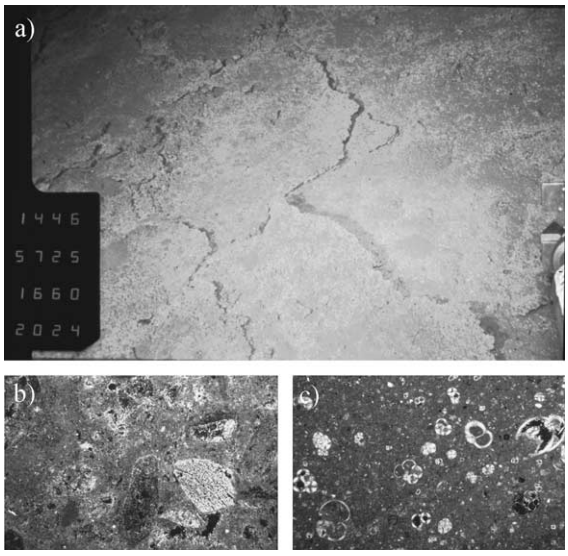

Fig. 2. In situ aspect (a) and thin-section photomicrographs (b,c) of carbonate crusts formed on eastern Mediterranean mud volcanoes. (a) Crust pavement outcropping on the Amsterdam mud volcano probably due to erosion and/or post emplacement remobilization of mudflows (crust polygons about 2 m across). (b) Typical texture of a mud breccia crust where sedimentary rock fragments are immersed in a fine-grained matrix/cement (polarized light, Kazan mud volcano). (c) Typical texture of a pelagic crust where tests of calcareous planktonic organisms are immersed in a fine-grained matrix/cement (polarized light).

Unconsolidated pelagic and mud breccia sediments sampled by coring during submersible dives provide

Table 1
Chemistry of the expelled fluids at the studied eastern Mediterranean cold seep sites

Site	Ca^{2+} (mM)	DIC (mM)	CH_4 (mM)
Napoli	0–0.54	28–52	0–120
Amsterdam	0.33	25	0–120
Kazan	0–5	3–15	0–120

The Ca^{2+} and DIC concentrations were determined on samples taken from the inferior parts of sediment cores and are unaffected by surface biogeochemical reactions. Data from De Lange and Brumsack (1998), Haese et al. (2003); Haese et al. (submitted for publication).

the reference isotope composition of carbonate materials prior to cementation.

Care was taken, when selecting samples of unlithified sediments and carbonate crusts for analysis, to exclude shells or shell fragments. Reference is made to Aloisi et al. (2000) for methods used to determine the carbonate content, mineralogy (XRD) and carbon stable isotope composition of unlithified sediments and carbonate crusts. XRD analysis showed a bimodal distribution of calcite $d(104)$ values suggesting the existence of two sources of calcite in unlithified sediments and carbonate crusts. A low-Mg source with $d(104)$ values centered around 3.028 Å derives from the carbonate tests of pelagic organisms and will be referred to as *calcite* in this paper. A second, authigenic, source with $d(104)$ values centered around 2.998 Å possibly contains up to 12 mol% Mg and will be referred to as *high-Mg calcite* in this paper.

The ^{14}C activity of authigenic carbonates and unlithified sediments was determined by liquid scintillation (Packard 2260 XL). The dates presented (Table 2) are normalized to a $\delta^{13}C$ of −25‰ PDB (Stuiver and Polach, 1977).

3. Stable and radiocarbon isotope results

The studied carbonate types can be discerned on the basis of their mineralogy and their $\delta^{13}C$ and ^{14}C content (Fig. 3, Table 2). The carbonate mineralogy and $\delta^{13}C$ of both pelagic and mud breccia sediments (~0‰ PDB) is in agreement with the predominance of calcitic tests of pelagic organisms in their carbonate fraction (Cita et al., 1996b). They differ considerably, however, in their ^{14}C content. Pelagic sediments contain 37.1% and 41% modern carbon (MC), corresponding to an apparent ^{14}C age of 8.2±0.1 and 7.2±0.1 ka, respectively. This is consistent with their provenance from the top 20 cm of the eastern Mediterranean pelagic succession that has a sedimen-

Table 2
Mineralogy and stable and radiogenic isotope composition of unlithified sediments and carbonate crusts from cold seeps of the eastern Mediterranean Sea

Sample (depth, cm)	Site[a]	Sample type[b]	$CaCO_3$ (wt.%)	Dominant carbonate[c]	Calcite (wt.%)	$D^{14}C$[d] (‰)	MC[e] (%)	$\delta^{13}C$ (‰ PDB)	Apparent ^{14}C age[f] (ka)
MN13BT8 (10)	A	PS	48	Ca	≈45	−628.7±4	37.1±0.4	−0.21	8.2±0.1
MN13CT3 (25)	A	PS	48	Ca	≈45	−589±5.3	41.0±0.5	−3.07	7.2±0.1
MNLGC11s3 (220)	A	MB	23	Ca	18	<−993.5	<0.7	−2.22	>40
MN12BT3 (0)	K	PC	83	Ca	75	−620.5±5	38.0±0.5	−20.55	7.8±0.1
MN13BT4 (0)	A	MBC	76	Ar/HMC	<5	−878.2±6	12.2±0.6	−20.4	17.4±0.4
MN16BT4 (0)	N	CH	85	Ar	0	−721.7±1	27.8±1	−23.15	10.2±0.3
MN14BT3 (0)	A	MBC	72.9	Ar	9	−945.0	5.5	−19.14	23.3±0.2
MN6BT1 (0)	N	MBC	85.2	Ar	9	−838.4	16.2	−16.63	14.6±0.1
MN10BT (0)	K	PC	91.2	HMC	25	−754.3	24.6	−24.94	11.3±0.2
MN4BT1 (0)	N	MBC	90	Ar	2	−899.0	10.1	−14.13	18.4±0.4
MN14BT7 (0)	A	MBC	85.6	Ar	8	−930.2	7.0	−27.52	21.4±0.2
MN6BT4 (0)	N	MBC	93.2	Ar	2	−872.5	12.7	−22.47	16.5±0.1

[a] A—Amsterdam mud volcano, K—Kazan mud volcano, N—Napoli mud volcano.
[b] PS—unlithified pelagic sediments, MB—unlithified mud breccia, PC—pelagic crust, MBC—mud breccia crust, CH—chemoherm.
[c] Ca—calcite, Ar—aragonite, HMC—high-Mg calcite.
[d] Per mil departure of the sample activity, corrected for isotope fractionation, from the activity of the modern standard.
[e] Percent modern carbon.
[f] ^{14}C-ages were calculated using a ^{14}C half-life of 5730 years.

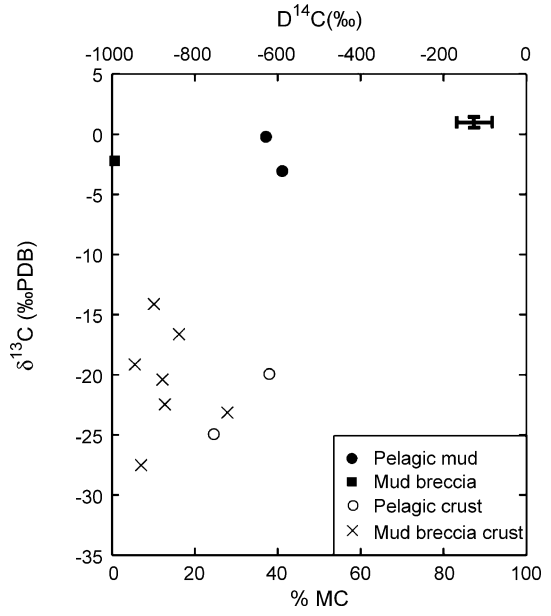

Fig. 3. Plot of $D^{14}C$ vs. $\delta^{13}C$ for carbonate materials from eastern Mediterranean cold seep settings. The horizontal and vertical bars represents the range of $D^{14}C$ and $\delta^{13}C$ of Mediterranean bottom water masses in the two studied areas, respectively (the $D^{14}C$ values were measured from living bivalves [see Section 4.3] and the $\delta^{13}C$ values were taken from Pierre, 1999).

tation rate of approximately 2 to 3 cm per 1000 years (Cita et al., 1996b). The mud volcanic deposit, instead, contains only trace amounts of ^{14}C (<0.65% MC) and is older than the limit of conventional ^{14}C-dating (35–40 ka), consistent with expulsion of deep sedimentary material (mud breccia).

Authigenic crusts, which are composed of a variety of carbonate minerals (aragonite, calcite and high-Mg calcite), combine ^{13}C depletion ($-27.52<\delta^{13}C$ ‰ PDB<-14.13) with a variable, but always significant, ^{14}C content ($5.5<$%MC<38.3). The carbonate crusts are significantly ^{13}C-enriched compared to biogenic or thermogenic methane ($-100<\delta^{13}C$ ‰ PDB<-30), indicating that an isotopically heavier carbon source is participating in their formation. Based on the amount of calcite in the crusts determined by XRD analysis (Table 2), it is clear that the very small amount of calcite of probable pelagic origin in crusts MN6BT4, MN4BT1 and MN13BT4 cannot account for all of the ^{13}C-enrichment of these crusts ($-22.47<\delta^{13}C$ ‰ PDB<-14.13) compared to methane. Studies of pore water chemistry at cold seeps (Paull et al., 1992) have shown that $\delta^{13}C_{DIC}$ values intermediate between those of methane and bottom water DIC are produced by mixing of these two sources in the top few centimeters of sediments. It is thus very likely that bottom waters provided an appreciable, albeit unknown, amount of DIC for the formation of the authigenic carbonates considered in this study. Pelagic crusts from Kazan mud volcano have the highest ^{14}C content (24.6% and 38.0% MC), comparable to that of modern pelagic sediments (see Table 2), suggesting that pelagic sediments supply an important part of the ^{14}C contained in these crusts. Because mud breccia contains virtually no ^{14}C, the source of ^{14}C in mud breccia crusts must lie in the authigenic carbonate cement. Methane, which is nearly always associated with mud volcanism and probably plays an important role in the overpressurisation of the mud (Brown, 1990), is of relatively deep origin and most likely is devoid of ^{14}C. Bottom water DIC is therefore the only possible source of ^{14}C for authigenic carbonate minerals in the studied setting.

No attempt has been made yet to understand the controls that the cold seep environment exerts on the ^{14}C content of carbonate crusts. In the next section, we introduce a numerical model that we use to gain insight into these controls.

4. Numerical modeling of crust formation

A numerical model was applied to simulate the formation of carbonate crusts at cold seeps and to investigate the factors affecting their ^{14}C content. The one-dimensional nonsteady-state model, based of the numerical treatment of early diagenetic processes of Berner (1980), is described in detail in the appendix. The model considers AMO and calcium carbonate precipitation, the two major reactions taking place at cold seeps (Luff and Wallmann, 2003). In addition, it considers a simple version of the DIC system and the decrease of porosity induced by calcium carbonate precipitation. The distribution of eight chemical species (CH_4, SO_4^{2-}, HCO_3^-, CO_2, Ca^{2+}, $H^{14}CO_3^-$, $CaCO_3$, and $Ca^{14}CO_3$) forced by advection, molecular diffusion, eddy diffusion, bioturbation, bioirrigation, convection, AMO, calcium carbonate precipitation and dissolution, and ^{14}C radioactive decay can be described.

We will briefly introduce the conceptual basis for the treatment of fluid chemistry when convection is considered in our model (see the appendix for the full mathematical treatment). Convection at cold seeps mixes seawater with deep fluids and increases the rate of fluid flow in the upper part of the fluid conduit (Henry et al., 1992). Considering a geometry of the convective cell comparable to the one proposed by Henry et al. (1992) (Fig. 4), we propose that convecting sulfate-rich and methane-free seawater mixes with deep, methane-rich and sulfate-free fluids. The resulting fluid mixture will be reactive. Methane will be oxidized by sulfate and part of the bicarbonate produced by this reaction will react with calcium forming calcium carbonate. The resulting chemistry at the base of the model column will depend on the extent to which these reactions will have advanced towards equilibrium before the fluids enter the model column. Thus, our model accounts for the presence of unreacted mixtures of methane and sulfate in cold seep fluids, a feature observed at a number of cold seep sites (Boetius et al., 2000; Luff and Wallmann, 2003; Hensen, personal communication).

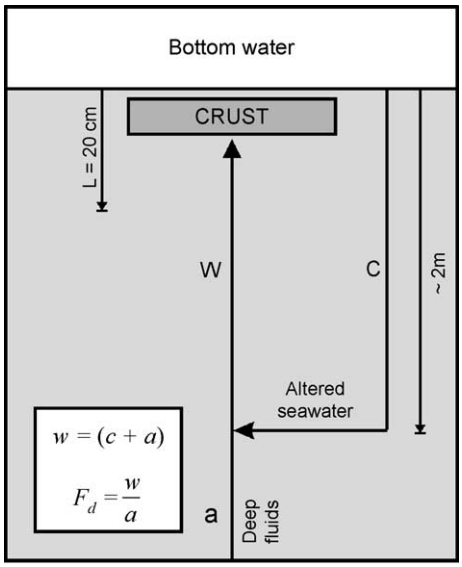

Fig. 4. Schematic representation of convection at cold seeps. Note that the size of the modeled sediment column is much smaller than the size of the convection cell. When convection is considered in the model, the initial advection rate at the surface is equal to the sum of the advection rate of deep fluids and the convection rate of seawater.

By acting on the hydrological, chemical and biological parameters of the model (Tables 4–6), the behavior of ^{14}C during crust formation can be investigated under a wide range of environmental conditions. We first illustrate the main features of the model describing a standard case of crust formation under conditions which likely are common at the eastern Mediterranean cold seep sites (Section 4.1). Then, we investigate the effect of varying single chemical, biological and hydrological parameters on the ^{14}C-content of the standard crust (Section 4.2). Finally, we use the model to reproduce the ^{14}C-content of some eastern Mediterranean carbonate crusts (Section 4.3), in order to investigate the environmental conditions active during their formation.

4.1. The formation of a 'standard' crust

The main features of the model will be illustrated describing the evolution of solute and solid concentrations, saturation state, AMO and $CaCO_3$ precipitation rates, porosity and advection during the formation of a model crust under the influence of diffusion and advection alone. The boundary conditions used in this model run (Table 3, for other parameters refer to Table A1) fall in the ranges of pore water fluid chemistry measured at the eastern Mediterranean cold seep sites (Table 1).

During the initial years of crust formation (t=0–10 years), advection approaches 10 cm year^{-1} (Fig. 5k). Upwards advecting and diffusing methane (Fig. 5b) overlaps with downwards diffusing sulfate (Fig. 5a) defining a reaction zone where AMO and production of bicarbonate occur (see appendix, Eq. (6)). The maximum rate of AMO (100 μmol cm^3 year^{-1}) occurs at the center of the reaction zone (about 6-cm depth, Fig. 5g) and results in maxima of bicarbonate concentration (Fig. 5c) and calcium carbonate supersaturation at roughly the same depth (Fig. 5h). Downwards diffusing calcium (Fig. 5d) reacts with bicarbonate producing calcium carbonate and initiating crust formation. Because the rate of calcium carbonate precipitation is proportional to the saturation state, a peak in the rate of calcium carbonate precipitation (14 μmol cm^3 year^{-1}) also occurs at this depth (Fig. 5i); it is thus the depth of the center of the AMO reaction zone that dictates the

Table 3
Set of boundary conditions used to illustrate crust formation (Section 4.1)

Parameter	Value
w	10 cm year^{-1}
BIO0	0 year^{-1}
xs	–
D_b0	0 cm^2 year^{-1}
xb	–
D_e0	0 cm^2 year^{-1}
xe	–
$CH_4(L)$	32 mM
$Ca^{2+}(L)$	5 mM
$HCO_3^-(L)$	15 mM
$CO_2(L)$	1.95 mM
$H^{14}CO_3^-(L)$	0 mM
$CaCO_3(0)$	5 wt.%
$CaCO_3(L)$	5 wt.%
$Ca^{14}CO_3(0)$	0 wt.%
$Ca^{14}CO_3(L)$	0 wt.%
f_{re}	0.918

See Tables A1 and A2 for explanation of symbols.

depth at which the crust is formed. AMO and carbonate precipitation (see appendix, Eqs. (3) and (6)) result in a net production of HCO_3^- and CO_2 (Fig. 5c,f). Because the neutral dissolved CO_2 molecule is surrounded by a smaller shield of water molecules than the charged HCO_3^- ion, CO_2 diffuses more rapidly than HCO_3^-. Consequently, undersaturation is produced in the upper part of the sediment column inducing dissolution. This feature of the model provides an additional explanation for the dissolution of carbonates at some cold seep sites, which was previously ascribed to CO_2 production through aerobic oxidation of methane (Matsumoto, 1990). $H^{14}CO_3^-$ penetrates the sediment by diffusion (Fig. 5e) and is incorporated in the precipitating $CaCO_3$ (Fig. 5l; note that concentrations of $H^{14}CO_3^-$ and $Ca^{14}CO_3$ are reported relative to those of HCO_3^- and $CaCO_3$, respectively, using the $D^{14}C$ notation). The shape of the pore water profiles is controlled by the transport-reaction processes which, at this stage, are not affected significantly by the small amount of authigenic carbonate formed; the solute concentrations are in a quasi-steady state.

As precipitation proceeds (t=500 years), porosity decreases (Fig. 5j) and both transport and reaction processes are affected. Advection at the bottom of the model column decreases as approximated by the $wt(t)$ function (see appendix, Eq. (18)), and an advection maximum is produced at the depth of the porosity minimum due to the Venturi effect (the increase in flow rate of a constrained fluid as the section perpendicular to flow is reduced; see appendix, Eq. (19); Fig. 5k). The diffusive flux of solutes across the crust decreases proportionally to the decrease in porosity and the increase in tortuosity. As a result, a barrier for solute transport is formed; Ca^{2+}, SO_4^{2-} and $H^{14}CO_3^-$ accumulate above the crust while CH_4, HCO_3^- and CO_2 accumulate below it. Solute concentration profiles steepen and the degree of carbonate saturation decreases (Fig. 5h). Due to the steepening of the $H^{14}CO_3$ pore water profile, pore water $H^{14}CO_3$ concentrations in the upper part of the crust increase (Fig. 5e), leading to an increase in the ^{14}C incorporated in the upper part of the crust (Fig. 5l). The rate of AMO decreases proportionally to the decrease in porosity (Fig. 5g). Conversely, due to the increase in $CaCO_3$ in the model column, the rate of calcite precipitation increases considerably after the initial years of crust formation, reaching a maximum of about 19 μmol cm^3 year^{-1} at 500 years (Fig. 5i).

When porosity is greatly decreased (t=950 years), the saturation state of pore fluids with respect to carbonate is strongly diminished (Fig. 5h) and the rate of calcium carbonate precipitation decreases (Fig. 5i). Following the steepening of solute concentration profiles, the maxima in the AMO and $CaCO_3$ precipitation rate profiles sharpen (Fig. 5g,i) and the small amount of solute transport is dominated by the Venturi effect (Fig. 5k). A crust formed under these conditions has a $D^{14}C$ of −916.7‰.

4.2. Controls on the ^{14}C content of crusts

Sets of model runs were performed varying separately chemical, biological and hydrological model parameters in order to understand the controls on the ^{14}C content of carbonate crusts (Tables 4–6). In any given set of runs, only one parameter was varied, while the others were kept the same as those used in the run for the standard crust (Table 3). Runs which consider convection are the only exception because this process affects the chemistry of the fluid at the lower boundary (see appendix). A number of runs were repeated omitting the decay

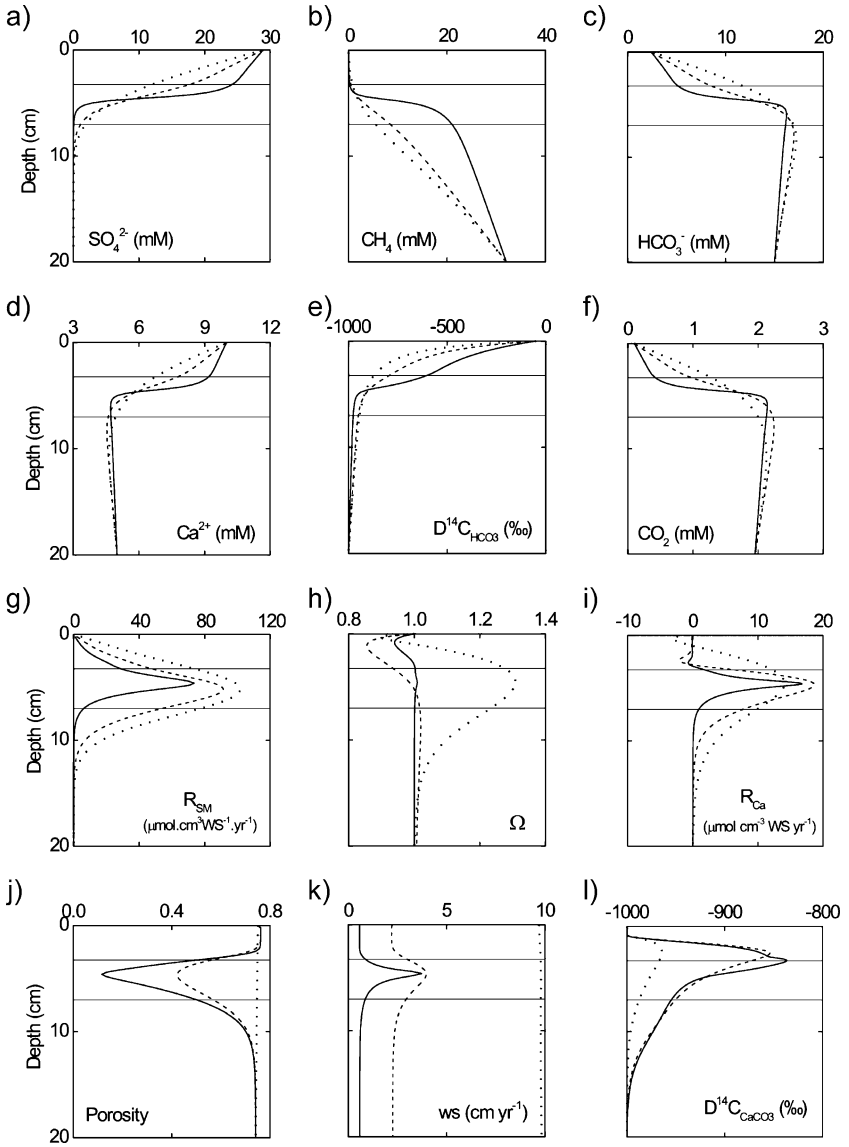

Fig. 5. Evolution of chemical and physical parameters during the formation of a model crust under the boundary conditions specified in Tables 3 and A1. Notes: dotted line, t=10 years; dashed line, t=500 years; solid line, t=950 years. The two horizontal lines correspond to the depth at which the porosity is equal to 0.5 and define the top and bottom of the crust.

term in the differential equation for $H^{14}CO_3^-$ in order to investigate the effect of time of crust formation on crust $D^{14}C$ (Table 4). The range of variation of chemical parameters was chosen based on chemical surveys of cold seeps from eastern Mediterranean mud volcanoes (Haese et al., 2003; Haese et al., submitted for publication), the Aleutian Trench (Wallmann et al., 1997) and Hydrate Ridge (Luff and Wallmann, 2003) where carbonate crusts have formed recently or are actively forming. The range of variation of some biological and hydrological parameters was chosen based on a recent model study of cold seep carbonate crust formation (Luff et al., 2004). Henry et al. (1992) estimate that density-driven convection on the Nankai Accretionary Prism results in dilution of deep fluids with

Table 4
Effect of the chemistry of seeping fluids on the $D^{14}C$ of carbonate crusts

$CH_4(L)$ (mM)	Ca^{2+} (mM)	$HCO_3^-(L)$ (mM)	$CO_2(L)$ (mM)	$D^{14}C$ crust (‰)	t_{max}[a] (year)	$D^{14}C$ crust[b] (‰)
16	5	15	1.95	−947.4	2100	−937.1
32	5	15	1.95	−922.5	950	−916.5
48	5	15	1.95	−906.8	620	−900.8
64	5	15	1.95	−892.9	450	−888.9
120	5	15	1.95	−883.3	250	−881.9
32	5	5	0.22	−903.8	1050	−896.9
32	5	15	1.95	−921.9	950	−926.5
32	5	25	5.43	−936.0	950	−931.3
32	5	35	10.63	−949.3	950	−945.3
32	5	55	26.26	−967.4	1100	−965.7
32	1	15	0.39	−905.5	800	−900.0
32	3	15	1.17	−912.9	900	−907.0
32	5	15	1.95	−919.9	950	−914.5
32	10	15	3.91	−933.9	1150	−928.5

[a] Simulation time needed to attain a minimum porosity in the sediment column of 0.1.
[b] $D^{14}C$ of the crust calculated omitting the ^{14}C-decay terms in the differential equations for the $H^{14}CO_3^-$ and $Ca^{14}CO_3$ species.

bottom waters by a factor of approximately 10. We have extended this range and investigated the effect of convection on the $D^{14}C$ of carbonate crusts considering a dilution of deep fluids with bottom waters of up to 15.

Table 5
Effect of biological parameters on the $D^{14}C$ of carbonate crusts

D_b0[a] (cm year^{-1})	xb[b] (cm)	BIO0[c] (year^{-1})	xs[d] (cm)	$D^{14}C$ crust (‰)	t_{max}[e] (year)
0.01	5	0	–	−921.7	1100
0.05	5	0	–	−932.0	1500
0.1	5	0	–	−935.6	1800
0.2	5	0	–	−940.0	2200
0.1	2	0	–	−913.1	1500
0.1	8	0	–	−940.7	3600
0	–	10	10	−920.3	1000
0	–	30	10	−922.5	900
0	–	50	10	−920.9	820
0	–	100	10	−919.7	750
0	–	30	1	−913.7	950
0	–	30	50	−930.7	750

[a] Bioturbation coefficient at the surface.
[b] Halving depth of bioturbation.
[c] Bioirrigation coefficient at the surface.
[d] Halving depth of bioirrigation.
[e] Simulation time needed to attain a minimum porosity in the sediment column of 0.1.

Table 6
Effect of hydrological parameters on the $D^{14}C$ of carbonate crusts

w[a] (cm year^{-1})	F_d[b] (–)	D_e0[c] (cm^2 year^{-1})	xe[d] (cm)	$D^{14}C$ crust (‰)	t_{max}[e] (year)
1	1	0	–	−917.9	1050
10	1	0	–	−914.9	950
30	1	0	–	−912.9	790
50	1	0	–	−913.5	650
100	1	0	–	−913.5	290
10	5 (6 mM)	0	–	−888.7	800
10	10 (6 mM)	0	–	−888.9	800
10	15 (6 mM)	0	–	−889.0	800
10	15 (8 mM)	0	–	−880.0	800
10	15 (10 mM)	0	–	−868.5	800
10	15 (15 mM)	0	–	−832.0	800
10	1	1000	5	−917.4	800
10	1	2000	5	−916.2	750
10	1	3000	5	−916.8	650
10	1	4000	5	−916.5	650
10	1	1000	2	−917.0	800
10	1	1000	8	−919.7	600

[a] Initial advection rate at the surface.
[b] Factor by which deep fluids are diluted by seawater during convection and residual sulfate at the lower boundary (in parenthesis). Changes in F_d affect also the lower boundary condition for solutes (see appendix).
[c] Eddy diffusion coefficient at the surface.
[d] Halving depth of eddy diffusion.
[e] Simulation time needed to attain a minimum porosity in the sediment column of 0.1.

Our results show that the considered chemical, biological and hydrological parameters control crust $D^{14}C$ by affecting one or more of the following variables:

(1) The ^{14}C content of pore water bicarbonate ($D^{14}CHCO_3^-$). For a crust forming at a given depth, the higher the $D^{14}CHCO_3^-$, the greater the $D^{14}C$ of the crust.
(2) The depth at which the crust forms. For a given pore water $D^{14}CHCO_3^-$ profile, crusts formed nearer to the seafloor will incorporate relatively more ^{14}C.
(3) The time needed to form the crust. Because $H^{14}CO_3^-$ incorporated in a crust is separated from the bottom water reservoir, it experiences radioactive decay. The greater the time needed to form the crust, the greater the ^{14}C lost through radioactive decay during crust formation, and the smaller the $D^{14}C$ of the crust.

A summary of how single chemical, biological and hydrological parameters affect the above-mentioned variables is given in Table 6 and a graphic representation of the $D^{14}C$ shifts which are produced by varying single parameters is given in Fig. 6a. Briefly, increased amounts of CH_4 and HCO_3^- in the deep fluids, as well as increased advection rates, dilute pore water $H^{14}CO_3^-$ with HCO_3^-, both due to HCO_3^- production through AMO and due to an increase in the HCO_3^- flux from below. Bioirrigation, eddy diffusion and convection, instead, introduce $H^{14}CO_3^-$ in the pore fluids. Increases in the CH_4 flux at depth, produced by an increase in $CH_4(L)$ or of the advection rate (w), push the AMO reaction zone upwards, resulting in a decrease in crust depth. On the contrary, increased amounts of HCO_3^- and Ca^{2+} in the rising fluids

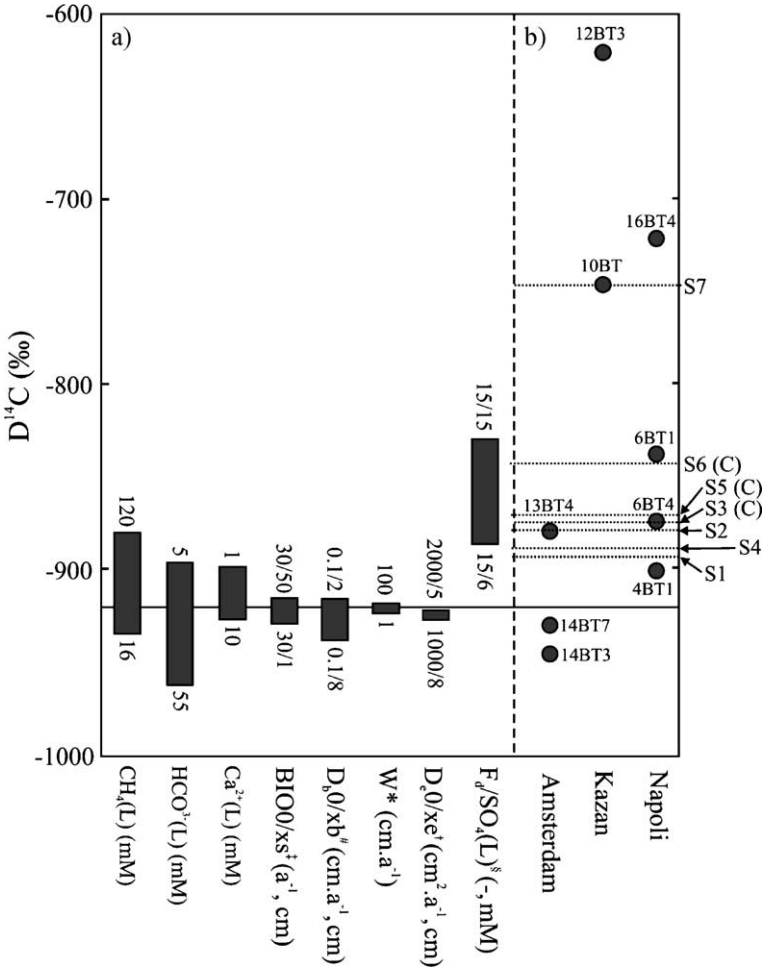

Fig. 6. (a) Deviations from the $D^{14}C$ of the standard crust (see Section 4.1) produced by varying single chemical, biological and hydrological parameters of the model. Bar graphs represent the range of $D^{14}C$ values obtained varying single parameters. The range of variation of each parameter is indicated at the extremities of each bar. The $D^{14}C$ of the standard crust is indicated by the horizontal line; (b) comparison between the ^{14}C-content of authigenic carbonate crust formed at cold seeps on eastern Mediterranean mud volcanoes (circles) with the ^{14}C-content of modeled crusts (dotted lines). Labels on the right of the dotted lines refer to model scenarios of Table 8. Sample names have been shortened by omitting the letters MN. Notes: (C) model scenario that considers convection; (‡) bioirrigation coefficient at the surface and halving depth of bioirrigation; (#) bioturbation coefficient at the surface and halving depth of bioturbation; (*) initial advection rate at the surface; (†) Eddy diffusion coefficient at the surface and halving depth of eddy diffusion; (§) factor by which deep fluids are diluted by seawater during convection and unreacted sulfate at the lower boundary.

Table 7
Summary of the influence of chemical, biological and hydrological parameters of the $D^{14}C$ of cold seep carbonate crusts

	Effect		
	Crust depth	$D^{14}C_{HCO_3^-}$	Crust $D^{14}C$
$CH_4(L)$	strong decrease	small decrease	increase
$HCO_3^-(L)$	small increase	small decrease	decrease
$Ca^{2+}(L)$	small increase	no effect	small decrease
w[a]	moderate decrease	moderate decrease	no effect
F_d[b]	no effect	moderate increase	small increase
$SO_4^{2-}(L)$[c]	no effect	increase	increase
D_e0[d]	increase	increase	no effect
xe[e]	increase	increase	no effect
BIO0[f]	moderate increase	moderate increase	no effect
xs[g]	strong increase	moderate increase	small decrease
D_b0[h]	increase	no effect	decrease
xb[i]	increase	no effect	decrease

[a] Initial advection rate at the surface.
[b] Factor by which deep fluids are diluted by seawater during convection.
[c] Unreacted sulfate at the lower boundary.
[d] Eddy diffusion coefficient at the surface.
[e] Halving depth of eddy diffusion.
[f] Bioirrigation coefficient at the surface.
[g] Halving depth of bioirrigation.
[h] Bioturbation coefficient at the surface.
[i] Halving depth of bioturbation.

increase the depth of maximum supersaturation and thus increase the depth of crust formation. Bioirrigation and eddy diffusion, by enhancing the SO_4^{2-} flux in the sediment and increasing the depth of the AMO reaction zone, result in a deepening of the crust. Runs omitting the ^{14}C-decay term show that the time needed to form a crust (not to be confused with the ageing of a formed crust) has only a minor influence on crust ^{14}C content. The effect that single model parameter variations have on crust $D^{14}C$ results from the combined effect that the parameter variations have on the variables 1 to 3, above (Table 7). The highest crust ^{14}C content is obtained in runs which consider convection (Fig. 6a). Interestingly, it is the amount of unreacted sulfate at the lower boundary (i.e. the extent to which the seawater-deep fluid mixture reacts through AMO) that exerts the strongest control on crust $D^{14}C$, rather than the dilution factor, F_d, between convecting seawater and deep fluids (Table 6). This is because AMO adds ^{14}C-free DIC to pore waters, diluting the seawater-derived ^{14}C, so that smaller amounts of AMO in the convecting cell, and thus higher amounts of unreacted sulfate at the lower boundary, result in increased crust $D^{14}C$.

Bioturbation transports authigenic carbonate downcore and results in a thicker crust. The time needed to form a crust increases, leading to a small decrease of crust $D^{14}C$ (Table 5).

4.3. Applying the model to the eastern Mediterranean crusts

A set of seven model runs (Table 8) was performed to investigate the chemical and hydrological conditions under which the eastern Mediterranean cold seep carbonate crusts discussed in Section 2 were formed. The ^{14}C content of Mediterranean crusts and the model results are compared in Fig. 6b. Pore water

Table 8
Scenarios of fluid chemistry and hydrological conditions used to reproduce numerically the $D^{14}C$ of carbonate crusts formed in the eastern Mediterranean mud volcanoes

Scenario	$CH_4(L)$ (mM)	$SO_4^{2-}(L)$ (mM)	$Ca^{2+}(L)$ (mM)	$HCO_3^-(L)$ (mM)	w[a] (cm year^{-1})	F_d[b] (–)	$D^{14}C$ crust (‰)
1	120	0	0.33	25	10	1	−895.0
2	120	0	0.33	5	10	1	−879.0
3[c]	120	6	6.02	18.19	10	15	−872.0
4	120	0	0.1	28	10	1	−888.3
5[c]	120	6	5.97	18.32	10	15	−870.0
6[c]	120	10	6.52	16.08	10	15	−845.0
7	120	0	0.1	12	10	1	−757.0

[a] Initial advection rate at the surface.
[b] Factor by which deep fluids are diluted by seawater during convection.
[c] See Table A5 for the complete definition of the chemistry at the lower boundary in runs which consider convection.

chemical data collected during the Medinaut and Medineth expeditions (Haese et al., 2003; Haese et al., submitted for publication) and during ODP Leg 160 (De Lange and Brumsack, 1998) provide the chemical composition of the seeping fluids (Table 1). In this set of runs, the crust $D^{14}C$ was calculated as the average $D^{14}C$ of the sediments that have a porosity smaller than 0.5, thus including the contribution from carbonates present in the sedimentary column prior to cementation. This formulation is necessary in order to account for ^{14}C-free carbonates in mud breccia and to consider ^{14}C-bearing modern pelagic carbonates in pelagic crusts. To account for a possible difference in ^{14}C content of the bottom water masses in the Olimpi and Anaximander zones, the factor accounting for the reservoir effect of water masses, f_{re} (see appendix), was determined for the two zones by measuring the ^{14}C activity of living bivalves collected during submersible dives (Medinaut cruise). An f_{re} of 0.918 (corresponding to a reservoir age of 680 years) was used to model crusts from the Olimpi area and an f_{re} of 0.818 (corresponding to a reservoir age of 1610 years) was used to model crusts from the Anaximander mountains area. The difference in reservoir age of the two considered water masses is likely due to the vicinity of the Olimpi area to the Aegean Sea which is the source of deep water formation in the eastern Mediterranean.

4.3.1. Amsterdam mud volcano

On the Amsterdam mud volcano, a calcium concentration of 0.33 mM and a DIC of 25 mM were measured in pore waters at sediment depths exceeding 1 m (Table 1). Imposing an advection rate, w, of 10 cm year^{-1}, $CH_4(L)$=120 mM and taking the previously cited $Ca^{2+}(L)$ and $HCO_3^-(L)$ values as lower boundary conditions, the modeled crust has a $D^{14}C$ of −895.0‰ (Table 7, scenario 1). Crusts MN14BT3 and MN14BT7, both from the Amsterdam dome, have a much smaller $D^{14}C$, equal to −945.0‰ and −930.2‰, respectively. Both these values can be reproduced with lower $CH_4(L)$, higher $HCO_3^-(L)$ or $Ca^{2+}(L)$, or a combination of the three. In addition, ageing can play a role, alone, or in combination with shifts in fluid chemistry, in decreasing crust $D^{14}C$. Crust MN13BT4 has a $D^{14}C$ of −878.2‰ (Table 2). This value can be attained if an $HCO_3^-(L)$ of 5 mM is imposed and all other boundary conditions of scenario 1 are applied (Table 7, scenario 2). Such a fluid chemistry, however, has not been observed on the Amsterdam mud volcano or at other cold seep sites, where low Ca^{2+} concentrations are generally coupled to high HCO_3^- concentrations (generally >15 mM; e.g. Wallmann et al., 1997; Luff and Wallmann, 2003). Alternatively, the elevated $D^{14}C$ of crust MN13BT4 is produced by convective mixing of bottom waters into the sediment. For example, with a seepage rate, w, of 10 cm year^{-1}, considering that convecting seawater mixes with the deep fluids of scenario 2 and that 6mM of sulfate are left unreacted at the lower boundary, with a dilution factor of deep fluids with seawater, F_d, of 15, the modeled crust has a $D^{14}C$ of −872‰ (Table 7, scenario 3).

4.3.2. Napoli mud volcano

On the Napoli mud volcano, low calcium concentrations, between 0 and 0.54 mM, and relatively high DIC concentrations, between 28 and 52 mM, have been measured (Table 1). The crusts sampled from this mud volcano have a wide range of ^{14}C-contents, from −899.0‰ to −721.7‰ (Table 2). A model crust formed with an $HCO_3^-(L)$ of 28 mM, a $Ca^{2+}(L)$ of 0.1 mM and a $CH_4(L)$ of 120 mM has a $D^{14}C$ of −883.3‰ (Table 7, scenario 4). The $D^{14}C$ of crusts MN4BT1 (−899.0‰) can be reproduced with lower $CH_4(L)$, higher $HCO_3^-(L)$ or $Ca^{2+}(L)$, or a combination of the three. Crust MN6BT4, however, has a $D^{14}C$ of −872.5‰, which is significantly higher than the modeled crust of scenario 4. A comparable ^{14}C content can be reproduced considering that convecting seawater mixes with the deep fluids of scenario 4 diluting them by a factor of 15 (Table 7, scenario 5) and that when the resulting fluid mixture reaches the lower boundary 6 mM of sulfate are left unreacted. Crust MN6BT1 has a $D^{14}C$ of −838.4‰. To approach its ^{14}C content, the chemistry of scenario 4 has to be coupled with convection allowing for a greater amount of unreacted sulfate (10 mM) at the lower boundary (Table 7, scenario 6). Crust MN16BT4, which was difficult to ascribe to either the mud breccia or the pelagic types based on sedimentological considerations, has a $D^{14}C$ of −721.7‰ (Table 2). This crust is thin (only 1–2 cm thick), has a high $CaCO_3$ content (85 wt.%) and its carbonate fraction is nearly entirely composed of aragonite (Table 2). Calcite is absent and high-Mg calcite is present in very low concentrations

(3 wt.%). The absence of calcite is hard to reconcile with the formation of this crust within the pore spaces of mud breccia or pelagic sediments, which always contain some pelagic carbonates. If pelagic material is not a source of ^{14}C, then the very high ^{14}C content implies that the crust formed very near, and possibly in contact with, the seawater ^{14}C source. Supplementary evidence for this is provided by the mineralogy of the crust. Because the sulfate ion inhibits the precipitation of calcite more than that of aragonite (Burton, 1993), the large predominance of aragonite confirms that this crust formed very near, or in contact with, bottom waters. Since AMO is required for the crust to form, conditions on the seafloor at this site have to be anoxic. Mineralogical and geochemical evidence suggests that at northern Hydrate Ridge massive aragonite build-ups form by precipitation from bottom waters (Teichert et al., 2003). These massive carbonate buildups, called chemoherms, possibly form due to the efficient O_2 removal near the seafloor carried out by mats of sulfide oxidizing bacteria (G. Bohrmann, private communication). Conditions such as these cannot be simulated with our model, where a saturation state with respect to calcite (Ω) of 1 is imposed as upper boundary condition, and transport processes are defined for the sedimentary porous medium. In any case, the hypothesis that crust MN16BT4 is a chemoherm-type carbonate is the most likely and explains both its mineralogy and its ^{14}C content.

4.3.3. Kazan mud volcano

On the Kazan mud volcano, measured calcium concentration in the rising fluids vary from 0 to 5 mM, and DIC concentrations from 3 to 15 mM (Table 1). Crust MN10BT has a $D^{14}C$ of −754.3‰ (Table 2) approaching that of crust MN16BT4 which we speculate is a chemoherm carbonate. However, a similar genesis for crust MN10BT seems highly unlikely since the main authigenic carbonate phase is high-Mg calcite and the crust contains 25 wt.% of calcite of probable pelagic origin. More likely, crust MN10BT is a pelagic crust. Assuming that the calcite present in this crust is indeed of pelagic origin, and that in calcite ^{14}C is present in the same concentration as in modern bottom waters of the Anaximander area, the ^{14}C content of this crust can be modeled. Such an elevated ^{14}C-content is reproducible numerically imposing an advection rate of 10 cm year^{-1}, using a calcium concentration of 0.1 and a DIC of 12 mM (Table 7, scenario 7). Similarly, the extremely high $D^{14}C$ of pelagic crust MN12BT3 (Table 2) is most probably due to the presence of calcite of pelagic origin, in very high amounts (75 wt.%), and was not modeled.

In summary, the elevated ^{14}C content of crusts MN13BT4, MN6BT4 and MN6BT1 can be realistically reproduced only allowing for the existence of convection. Given that we impose a $CH_4(L)$ of 120 mM in all simulations, which maximizes the ^{14}C content of the modeled crusts, we consider that our results strongly argue in favor for the existence of convection at the studied eastern Mediterranean cold seep sites. Various mechanisms have been proposed to explain convection at cold seeps; they will be discussed in the following section in the context of the eastern Mediterranean cold seep settings.

5. Discussion and conclusion

Density-driven convection takes place as a response of the density gradient produced between the expelled fluids and seawater by the upward flow of low-salinity and/or relatively warm pore fluids (Henry et al., 1992). The density gradient triggers lateral inflow of fluids into the conduit and results in downflow at their periphery, and convection. Given that the fluids expelled from the Napoli mud volcano are hypersaline and have a density of over 1.2 g cm^{-3} (De Lange and Brumsak, 1998), independently of the temperature of the expelled fluids, density-driven convection cannot be active on the Napoli mud volcano. Pore fluids expelled from the Kazan and Amsterdam mud volcanoes, however, have a salinity of only 20‰ at a depth of 30 and 120 cm, respectively so that convection is likely to occur. The Rayleigh criterion provides a simple means of checking if density-driven convection is possible at a given site. According to this criterion, for convection in a permeable horizontal layer to take place, the Rayleigh number, Ra, has to be greater than 10, provided that the fluid is allowed to flow freely through the upper boundary. For salinity-driven convection:

$$R_a = \frac{\varrho g \alpha_c \Delta S H k}{\mu D_c} \tag{28}$$

where ϱg is the hydrostatic pressure gradient (10^4 Pa m^{-1}), α_c is the coefficient relating salinity and density variations at a given temperature (0.75 at 13 °C, de Marsily, 1981), ΔS is the salinity contrast between seeping fluids and seawater (about 15‰ for the Amsterdam and Kazan mud volcanoes), H is the characteristic size of the system in m, k is the permeability in m^2, μ is the viscosity of water (approximately 10^{-3} Pa s), D_c is the diffusivity of the solute ($D_c=d_0+\beta|U_D|$). d_0, the molecular diffusivity, is about 10^{-9} m^2 s^{-1}, β, the coefficient of dispersivity is probably between 1 and 10 cm (Henry et al., 1992) and U_D is the Darcy velocity in m s^{-1} (equivalent to the rate of upwards fluid flow, w, in our model).

Imposing a salinity contrast of 15‰ and an advection rate of 10 cm $year^{-1}$ in Eq. (25), an Ra of 10 is exceeded if the permeability of the sediments in the conduit is greater than 10^{-16} m^2. The permeability of mud volcano sediments can vary considerably (~10^{-19}–10^{-15} m^2; Henry et al., 1996; Kopf et al., 1998). Henry et al. (1996) show that in mud volcano sediments the permeability of mud is proportional to its porosity; highly porous, fluid mud being the most permeable. Porosity measurements on samples obtained during ODP Leg 160 show that surface sediments of eastern Mediterranean mud volcanoes have porosities of up to 70%. Porosity measurements on surface samples obtained by gravity coring show even greater porosities (~80%; Haese et al., 2003). Based on the porosity–permeability relationship presented in Henry et al. (1996), a permeability of about 10^{-15} m^2 can be expected for surface mud of eastern Mediterranean mud volcanoes. Clearly, salinity-driven convection cannot be ruled out on the basis of the Rayleigh criterion alone. In fact, according to this criterion, convection is likely to occur at the cold seep sites on the Amsterdam and Kazan mud volcanoes. Furthermore, Henry et al. (1996) observe that convection in surface mud volcano sediments can be associated to expulsion of fluids along high permeability conduits, a scenario which cannot be excluded for the eastern Mediterranean sites too.

Two other mechanisms that produce convection at cold seeps involve the movement of a methane gas phase. The entrainment of fluid in a gas flow (O'Hara et al., 1995) may lead to inflow in adjacent sediments on a scale of a few meters. More recently, Tryon et al. (1999) proposed that the filling and emptying of subsurface gas reservoirs may also drive refluxing on a larger scale at Hydrate Ridge. Both these processes involve the presence of bubbles of free gas moving upwards in the sediment. No gas venting has been observed at the eastern Mediterranean cold seep sites during dives with the Nautile submersible in 1998. However, seafloor observations at Hydrate Ridge showed that gas venting can occur intermittently with intervals between activity periods of up to days, so that neither of the two processes above can be ruled out for the eastern Mediterranean sites. In particular, convection driven by entrainment in a gas flow or by the filling and emptying of subsurface gas reservoirs could possibly explain the extremely high ^{14}C contents of crusts from the Napoli mud volcano, where density-driven convection can be ruled out on the basis of the very high density of the seeping brines.

Regardless of the driving mechanism, our results strongly suggest that convection is responsible for providing an important amount of ^{14}C to some crusts. If convection is taking place on eastern Mediterranean mud volcanoes, it should result in an appreciable pore water chemical signature. Pore water profiles of dissolved sodium and boron in core MNLPC10 from the Kazan mud volcano show that the uppermost 70–90 cm of sediments contains seawater-like fluids (Fig. 7). Although it cannot be excluded that such profiles are produced by bioirrigation, the depth affected by inflow of seawater-like fluids is rather large for this process. Alternatively, such profiles could represent the chemical signature of shallow convection cells, such as those proposed by Henry et al. (1992). More field studies are needed to investigate the pore water chemical signature of shallow convection. In partic-

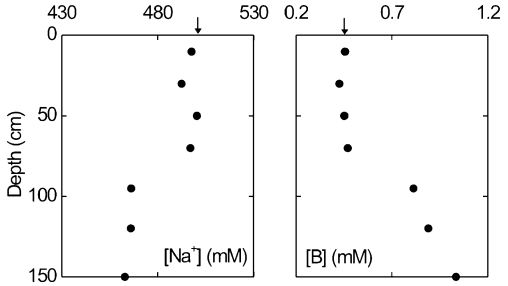

Fig. 7. Pore water concentration profiles of Na and B at the Kazan mud volcano showing inflow of seawater to a depth of 90 cm. Arrows show the Mediterranean bottom water concentration of Na and B.

ular, profiles similar to the ones in Fig. 7, but showing a deeper penetration of seawater-like fluids, would strongly argue in favor of convection, rather than bioirrigation.

Our modeling approach provides ample evidence for a linkage between chemical, biological and hydrological parameters of the cold seep environment and the concentration of the ^{14}C tracer in carbonate crusts. By controlling crust depth and the ^{14}C concentration in pore waters, the single parameters of the cold seep environment affect crust $D^{14}C$ in characteristic ways. In addition to the CH_4 concentration of the expelled fluids, convection is the only process capable of producing elevated ^{14}C concentrations in carbonate crusts. Fitting the ^{14}C field data from the eastern Mediterranean cold seeps provides strong support for the existence of convection at some of those sites and supports previous hypotheses that this process is widespread at cold seeps worldwide (Henry et al., 1996). The extension of our approach to the understanding of the behavior of other tracers at cold seeps such as stable carbon and oxygen isotopes, as well as trace elements, may provide more constrains on the processes taking place at modern cold seeps and, possibly, may provide some information on the chemistry and hydrology of ancient cold seeps.

Acknowledgments

Part of this work was carried out in the framework of the Medinaut project funded by IFREMER, the CNRS and NWO. The modeling work has been developed in the framework of the KOMEX and LOTUS research programmes financed by BMBF. The captains and crew members of the research vessel *Nadir* and of the *Nautile* provided helpful assistance at sea, their work is greatly appreciated. We are grateful to Marta Torres and Carolyn Ruppel for having provided constructive reviews of the manuscript. **[LW]**

Appendix A

The constant parameter values used to simulate the formation of carbonate crusts at the eastern Mediterranean cold seep sites are summarized in Table A1.

Table A1
Constant and variable parameter values used to describe the eastern Mediterranean sites and to investigate the controls on carbonate crust ^{14}C content

Parameter	Symbol	Value	Unit
Constant parameters			
Temperature	T	13	°C
Sedimentation rate	v_f	1×10^{-5}	cm year^{-1}
Porosity at sediment surface	ϕ_0	0.75	–
Porosity at great sediment depth	ϕ_f	0.7	–
Porosity depth attenuation coeff.	ϕ_a	0.01	cm^{-1}
Average density of solids	d_s	2.6	g cm^{-3}
Density of calcium carbonate	d_s^{Ca}	2.6	g cm^{-3}
Decay constant of ^{14}C	λ	1/8033	year^{-1}
Kinetic constant for AMO	k_{SM}	10	cm^3 μmol^{-1} year^{-1}
Kinetic constant for calcite precip.	k_{Ca}	0.1	year^{-1}
Solubility constant for calcite	K_{sp}	see text	(μmol cm^{-3})^2
$^{14}C/^{12}C$ in modern (pre-bomb) C	r_{14}	$1.2\cdot10^{-12}$	–
Length of the model column	L	20	cm
Diffusion coefficient for SO_4^{2-a}	$D_{SO_4^{2-}}$	234.15	cm^2 year^{-1}
Diffusion coefficient for CH_4[a]	D_{CH_4}	377.96	cm^2 year^{-1}
Diffusion coefficient for Ca^{2+a}	D_{Ca2}	175.76	cm^2 year^{-1}
Diffusion coefficient for HCO_3^{-a}	$D_{HCO_3^-}$	256.06	cm^2 year^{-1}
Diffusion coefficient for CO_2[a]	D_{CO_2}	402.12	cm^2 year^{-1}
Variable parameters			
Bioturbation coefficient at the surface	D_b0	variable	cm^2 year^{-1}
Halving depth of bioturbation	xb	variable	cm
Bioirrigation coefficient at the surface	BIO0	variable	year^{-1}
Halving depth of bioirrigation	xs	variable	cm
Eddy diffusion coefficient at surface	D_e0	variable	cm^2 year^{-1}
Halving depth of eddy diffusion	xe	variable	cm
Initial advection rate at the surface	w	variable	cm year^{-1}
Dilution factor due to convection	F_d	variable	–
Factor accounting for reservoir effect	f_{re}	variable	–

[a] Diffusion coefficients taken from Boudreau (1997).

Table A2
Boundary conditions used in the model

Species	Equation	Value	Unit
CH_4	$C_{CH_4}(0,t)=CH_4(0)$	0	μmol cm^{-3}
		variable	μmol cm^{-3}
	$C_{CH_4}(L,t)=10e^{\left[\frac{(L-10)}{8}\right]}-10e^{\left[\frac{10}{8}\right]}$		
SO_4^{2-}	$C_{SO_4^{2-}}(0,t)=SO_4^{2-}(0)$	28.9	μmol cm^{-3}
	$C_{SO_4^{2-}}(L,t)=SO_4^{2-}(L)$	variable	μmol cm^{-3}
Ca^{2+}	$C_{Ca^{2+}}(0,t)=Ca^{2+}(0)$	10	μmol cm^{-3}
	$C_{Ca^{2+}}(L,t)=Ca^{2+}(L)$	variable	μmol cm^{-3}
HCO_3^-	$C_{HCO_3^-}(0,t)=HCO_3^-(0)$	2.4	μmol cm^{-3}
	$C_{HCO_3^-}(L,t)=HCO_3^-(L)$	variable	μmol cm^{-3}
CO_2	$C_{CO_2}(0,t)=CO_2(0)$	0.1	μmol cm^{-3}
		variable	μmol cm^{-3}
	$C_{CO_2}(L,t)=\frac{Ca^{2+}(L)HCO_3^-(L)^2}{K_{sp}}$		
$H^{14}CO_3^-$	$C_{H^{14}CO_3^-}(0,t)=f_{re}HCO_3^-(0)r_{14}$	variable	μmol cm^{-3}
	$C_{H^{14}CO_3^-}(L,t)=H^{14}CO_3^-(L)$	variable	μmol cm^{-3}
$CaCO_3$	$C_{CaCO_3}(0,t)=CaCO_3(0)$	variable	wt.% dry sedim.
	$C_{CaCO_3}(L,t)=CaCO_3(L)$	variable	wt.% dry sedim.
$Ca^{14}CO_3$	$C_{Ca^{14}CO_3}(0,t)=f_{re}Ca^{14}CO_3(0)r_{14}$	variable	wt.% dry sedim.
	$C_{Ca^{14}CO_3}(L,t)=f_{re}Ca^{14}CO_3(L)r_{14}$	variable	wt.% dry sedim.

A number of hydrological, chemical and biological parameters were varied in successive experiments to investigate the controls on the ^{14}C content of carbonate crusts (Tables A1 and A2). The depth and time evolution of solid and solute concentrations is described by a set of eight transport-reaction differential equations, one for each chemical species considered in the model, and is constrained numerically by the chosen parameter values. The differential equations for dissolved species (Eq. (1)) and solids (Eq. (2)) are based on the general diagenetic equations of Berner (1980):

$$\frac{\partial(\phi(x,t)C)}{\partial t} = \frac{\partial}{\partial x}\left((D+D_e(x))\phi^2(x,t)\frac{\partial C}{\partial x}\right) + ws(x,t)\phi(x,t)\frac{\partial C}{\partial x} + \phi(x,t)BIO(x)(C_0-C) + \phi(x,t)\sum R_d(x,t) \quad (1)$$

$$\frac{\partial(1-\phi(x,t))C}{\partial t} = \frac{\partial}{\partial x}\left(D_b(x)(1-\phi(x))\frac{\partial C}{\partial x} - (1-\phi_f)v_f C\right) + (1-\phi(x,t))\sum R_s(x,t) \quad (2)$$

where C_d is the concentration of solutes in μmol (cm^3 pore fluids)$^{-1}$ (hereafter μmol cm^{-3}), C_s is the concentration of solids in weight percent dry sediment (hereafter wt.% DS), D, in cm^2 $year^{-1}$, is the molecular diffusion coefficient, and $\sum R_d$, in μmol (cm^3 pore fluid)$^{-1}$ $year^{-1}$ (hereafter μmol cm^{-3} $year^{-1}$) and $\sum R_s$, in wt.% DS $year^{-1}$, are the rates of all diagenetic reactions affecting dissolved and solid species, respectively. The reaction terms are defined in Table A3.

The system of eight differential equations is solved simultaneously using finite difference techniques as implemented in the commercial software MATHEMATICA. The vertical resolution of the modeling grid was set to 100 layers (i.e. 2-mm thickness of each layer). Choosing a higher resolution did not change the model results. The object NDSolve which was applied to integrate the differential equations uses the numerical Method of Lines. This procedure based on partial discretization has been used successfully in previous modeling of benthic processes (Boudreau, 1996; Boudreau, 1997; Luff et al., 2000). A typical model run was completed within 50 min of computation time on a PC with Pentium IV processor.

Starting from the initial concentration profiles for solutes and solids, quasi-steady-state concentrations for solutes are approached in less than 5 years of

Table A3
Reaction terms used in the differential equations for solute (Eq. (1)) and solute (Eq. (2)) concentrations

Species	Reaction term
CH_4	$\sum R_{CH_4}(x,t)=-R_{SM}(x,t)$
SO_4^{2-}	$\sum R_{SO_4^{2-}}(x,t)=-R_{SM}(x,t)$
Ca^{2+}	$\sum R_{Ca^{2+}}(x,t)=-f_{Ca}(x,t)R_{Ca}(x,t)$
HCO_3^-	$\sum R_{HCO_3^-}(x,t)=+R_{SM}(x,t)-2f_{Ca}(x,t)R_{Ca}(x,t)$
$H^{14}CO_3^-$	$\sum R_{H^{14}CO_3^-}(x,t)=-2f_{Ca}(x,t)R_{14_{Ca}}(x,t)-\lambda C_{H^{14}CO_3^-}(x,t)$
CO_2	$\sum R_{CO_2}(x,t)=+f_{Ca}(x,t)R_{Ca}(x,t)$
$CaCO_3$	$\sum R_{CaCO_3}(x,t)=R_{Ca}(x,t)$
$Ca^{14}CO_3$	$\sum R_{CaCO_3}(x,t)=R_{14_{Ca}}(x,t)-\lambda C_{H^{14}CO_3^-}(x,t)$

simulation time. However, as the crust builds and porosity decreases, both solid and solute concentrations are affected and steady state is attained only after very long simulation times. We have chosen to stop the model when a minimum porosity of 0.1 is attained. Although some cold seep carbonate crusts are probably less porous (Ritger et al., 1987), in other cases an appreciable porosity remains (Hovland et al., 1987). A value of 0.1 is a good numerical compromise given that smaller porosities result in steeper solute concentration gradients that need up to days of computation time to be correctly represented. In any case, the minimum porosity value has only a minor effect on the $D^{14}C$ of the crust. For a crust formed under the conditions listed in Table 3, for example, the $D^{14}C$ varies only from 917.2‰ to 916.1‰, as the minimum porosity of the crust varies from 0.28 to 0.06. The simulation time needed to attain a porosity of 0.1 varies, depending on the chemical and hydrological conditions used in our simulations, from 250 to 3600 years. At the end of each run, the $D^{14}C$ of the crust is calculated as the average $D^{14}C$ of the sediments that have a porosity smaller that 0.5. In the eastern Mediterranean, lithification decreases regularly from the top of the crust to the underlying sediment. Single crust samples considered in this study include the upper, well-lithified parts of crusts, as well as portions of their poorly lithified lower parts. A minimum porosity value of 0.5 was chosen to account for the apparent wide porosity range of our samples, and although this choice is rather arbitrary, the change in $D^{14}C$ produced if a different value of porosity is used is not large. For example, for the same crust considered above, as the porosity limit is changed from 0.5 to 0.2, the $D^{14}C$ changes only from −916.7‰ to −913.6‰.

A.1. DIC system, carbonate precipitation and porosity

The model considers a simplified version of the DIC system and calcium carbonate precipitation/dissolution processes which are described by the following reaction:

$$Ca^{2+} + 2HCO_3^- \Leftrightarrow CaCO_3 + CO_2 + H_2O \quad (3)$$

The degree of carbonate saturation, Ω, is expressed by:

$$\Omega = \frac{C_{Ca^{2+}}(x,t)C^2_{HCO_3^-}(x,t)}{C_{CO_2}(x,t)K_{sp}} \quad (4)$$

where K_{sp}, the solubility constant for calcite in seawater, is formulated in such a way that at the upper boundary Ω=1 and no precipitation or dissolution takes place:

$$K_{sp} = \frac{Ca^{2+}(0)HCO_3^-(0)^2}{CO_2(0)} \quad (5)$$

The rising fluids are considered to be in equilibrium with solid calcium carbonate, which is a realistic assumption given that they have moved through carbonate bearing sediments. The lower boundary condition for CO_2 is thus formulated in such a way that Ω=1 also at the lower boundary (Table A2).

Bicarbonate is produced through anaerobic oxidation of methane:

$$CH_4 + SO_4^{2-} = HCO_3^- + HS^- - + H_2O \quad (6)$$

The rate equation of this reaction is formulated following Van Cappellen and Wang (1996), where the rate, R_{SM}, is proportional to the concentration of both methane and sulfate:

$$R_{SM}(x,t) = k_{SM}C_{SO_4^{2-}}(x,t)C_{CH_4}(x,t) \quad (7)$$

The value of the kinetic constant for AMO, k_{SM}, was set to 10 $cm^3\ \mu mol^{-1}\ year^{-1}$. Although a wide range of k_{SM} values is reported in the literature (Van Cappellen and Wang, 1996), this value lies in the center of that range.

The rate of calcium carbonate precipitation, R_{Ca}, is assumed to depend linearly on saturation state and is defined to be proportional to the amount of calcium carbonate present in the sediment column (Hales and Emerson, 1997):

$$R_{Ca}(x,t) = k_{Ca}C_{CaCO_3}(x,t)(\Omega(x,t) - 1) \quad (8)$$

The value of the kinetic constant for calcium carbonate precipitation, k_{Ca}, was set to 0.1 $year^{-1}$. Repeated model runs showed that this k_{Ca} value produced a realistic saturation state (Ω=1.5–2) which has also been observed and simulated at other cold vent sites (Luff and Wallmann, 2003). In order for the

value of R_{Ca} computed in Eq. (8) to be used in the differential equations for dissolved species (Eq. (1)), its units have to be converted from wt.% $CaCO_3$ $year^{-1}$ to μmol cm^{-3} $year^{-1}$ considering the porosity change due to $CaCO_3$ precipitation, using the conversion function f_{Ca} (Table A4).

Due to their fine-grained nature, shallow mud volcano deposits have a high porosity, similar to that of clayey sediments. The initial porosity–depth distribution in the unlithified mud breccia sediment is considered to be produced by steady-state compaction (Berner, 1980) and is described by the following exponential function:

$$\phi(x,0) = \phi_f + (\phi_0 - \phi_f)e^{[-\phi_a x]} \quad (9)$$

where values of porosity at the sediment surface (ϕ_0) and porosity at great sediment depth (ϕ_f) are slightly smaller, and values of the porosity–depth attenuation coefficient (ϕ_a) slightly greater (Table A1) than those of fine-grained deep sea sediments to account for the provenance of the expelled muds from deep sedimentary intervals, and for a non-complete expansion of the sediment following expulsion and load removal.

The variation of porosity produced by precipitation and dissolution of calcium carbonate is taken into account by the following function:

$$\phi(x,t) = \phi(x,0) - (C_{CaCO_3}{}^*(x,t) - CaCO_3{}^*(0)) \quad (10)$$

where the asterisk denotes concentrations in cm^3 $CaCO_3$ per cm^3 of wet sediment. In order for the porosity changes to be computed correctly, calcium carbonate concentrations calculated by the model in wt.% of dry sediment are converted into units of cm^3 $CaCO_3$ per cm^3 of wet sediment applying the conversion factor f_{CaCO_3} (Table A4):

$$C_{CaCO_3}{}^*(x,t) = f_{CaCO_3} C_{CaCO_3}(x,t) \quad (11)$$

Substituting Eq. (11) in Eq. (10), solving for porosity and rearranging, we obtain:

$$\phi(x,t) = \frac{CaCO_3(0) - C_{CaCO_3}(x,t) + 100\phi(x,0)}{100 + CaCO_3(0) - C_{CaCO_3}(x,t)} \quad (12)$$

Values of porosity obtained with this function are used in the differential equations (Eqs. (1) and (2)).

A.2. Presence of ^{14}C and its decay

In order to understand the factors affecting the ^{14}C content of authigenic carbonates, the $H^{14}CO_3^-$ and $Ca^{14}CO_3$ species have been introduced in the model and are allowed to be transported and to react independently of HCO_3^- and $CaCO_3$. In our simplified treatment of the DIC system, all the ^{14}C is contained in bicarbonate. The upper boundary value for the concentration of $H^{14}CO_3^-$ can therefore be obtained by:

$$H^{14}CO_3^-(0) = f_{re} r_{14} HCO_3^-(0) \quad (13)$$

where r_{14}, the $^{14}C/^{12}C$ abundance ratio in modern (pre-bomb) carbon, is equal to 1.2×10^{-12} (Kutschera,

Table A4
Unit conversion functions and factors used in the numerical model

Parameter	From units	To units	Function/factor
R_{Ca}	wt.% $CaCO_3$ $year^{-1}$	μmol cm^{-3} $year^{-1}$	$f_{Ca}=\frac{10d_s(1-\phi_{(x,t)})}{0.1\phi_{(x,t)}}$
C_{H14CO_3-}	μmol cm^{-3}	‰	$D^{14}CHCO_3^- = \left(\frac{C_{H^{14}CO_3^-}}{C_{HCO_3^-} r_{14}} - 1\right)1000$
C_{Ca14CO_3}	wt.%	‰	$D^{14}CCaCO_3 = \left(\frac{C_{Ca^{14}CO_3}}{C_{CaCO_3} r_{14}} - 1\right)1000$
C_{CaCO_3}	wt.%	cm^3 $CaCO_3$ cm^{-3} WS	$f_{CaCO_3} = \frac{d_s(1-\phi_{(x,t)})}{100 d_s^{Ca}}$

2000) and the factor f_{re} accounts for the reservoir effect of eastern Mediterranean bottom waters. The value of f_{re} is obtained by substituting the reservoir age in years in the equation for the conventional radiocarbon age:

$$t = -8033\ln\left[1+\frac{D^{14}C}{1000}\right] \quad (14)$$

This expression is then solved for $D^{14}C$ and the value obtained is substituted, with Eq. (13), in the expression for $D^{14}C$ (Table A4). When investigating the controls on crust ^{14}C contents (Section 4.2), an f_{re} of 0.918 was used, which corresponds to the reservoir effect of bottom waters in the Olimpi area. The lower boundary condition for $H^{14}CO_3^-$ is always zero except when convection introduces ^{14}C-bearing bottom waters in the sediment column (see below).

^{14}C decay is treated as a homogeneous reaction with first order rate law (Berner, 1980):

$$\frac{\partial C}{\partial t} = \lambda C \quad (15)$$

where C is the concentration of either $H^{14}CO_3^-$ or $Ca^{14}CO_3$ and λ is the (first order) decay constant of ^{14}C. The decay term (λC) is introduced in the reaction terms of the differential equations for the $H^{14}CO_3^-$ and $Ca^{14}CO_3$ species (Table A3). $H^{14}CO_3$ and $Ca^{14}CO_3$ concentrations are converted from μmol cm^{-3} and wt.% to the more standard per mil notation using the equation shown in Table A4.

In order to account for variations in the ^{14}C concentration of dissolved bicarbonate during dissolution, a separate expression for the rate of carbonate precipitation was used in the differential equations for $H^{14}CO_3$ and $Ca^{14}CO_3$:

$$R^{14}_{Ca}(x,t) = H[R_{Ca}(x,t)]R_{Ca}(x,t)\frac{C_{H^{14}CO_3}(x,t)}{C_{HCO_3}(x,t)} + H[-R_{Ca}(x,t)]R_{Ca}(x,t) \times \frac{C_{Ca^{14}CO_3}(x,t)}{C_{CaCO_3}(x,t)} \quad (16)$$

where H, the Heaviside function, is equal to 0 if its argument is negative, and equal to 1 if its argument is equal to 0 or is positive. Like the R_{Ca} expression used in the differential equations for the non-radiogenic chemical species (Eq. (8)), the expression allows for dissolution of carbonate when R_{Ca} is negative and precipitation of carbonate when R_{Ca} is positive. In addition, it correctly computes the changes in isotopic composition of dissolved bicarbonate and solid carbonate during these processes.

A.3. Transport processes

The numerical description of diffusion, advection, bioirrigation and bioturbation processes is based on the general diagenetic equations of Berner (1980).

Molecular diffusion coefficients for the solute species (Table A1) are taken from Boudreau (1997). If bottom currents are sufficiently intense, solute concentration profiles can be affected by bottom current stirring (Berner, 1980). To investigate the effect of this process on the ^{14}C of carbonate crusts, we introduced a depth-dependent eddy diffusion coefficient, $D_e(x)$, in the differential equations for solutes (Eq. (1)):

$$D_e(x) = D_e 0\exp\left[\frac{x^2}{2xe}\right] \quad (17)$$

where xe, in cm, is the halving depth of eddy diffusion.

Because fine-grained sediments undergo compaction soon after sedimentation, the advection of solids at a given depth (i.e. the velocity of downwards flow of bulk solids relative to the seafloor) is equal to the rate of burial, or sedimentation rate, v_f, modified by compaction (Berner, 1980). The formulation used in the differential equations is valid for steady-state compaction (Berner, 1980). Mineralogical and petrographic evidence (Aloisi et al., 2000) suggests that the mud breccia crusts considered in this study do not include recent pelagic sediments in their upper parts, suggesting either that they form very rapidly after the emplacement of a mudflow, so that pelagic material accumulating on the mudflow is not included in the crust, or that portions of the mud volcanoes are swept by bottom currents that inhibit sedimentation. A low sedimentation rate was chosen to reproduce the absence of pelagic sediments in the upper part of mud breccia crusts.

Since in our case the upward component of fluid advection due to seepage (w) is much greater than the downward component resulting from burial and compaction processes, the effect of burial and compaction on the advection of fluids has been

neglected in the model. The effect of precipitation- and dissolution-induced porosity variations on fluid flow rates, instead, has to be taken into account. If the advective flux of fluids through the sediment column is constant during crust formation and no lateral fluid flow is possible, the rate of upward fluid flow will increase as calcium carbonate precipitation decreases porosity (Venturi effect). In reality, however, as the permeability decreases with falling porosity, a part of the fluids will use lateral conduits of higher permeability and will be expelled in portions of the seafloor not covered by crusts. Eventually, when a crust is well established and carbonate cements nearly entirely fill the pore spaces, fluid flow through the crust will come to an end. In the model, both the lateral fluid flow and the Venturi effect are tentatively simulated. A time dependence of fluid flow is introduced to account for the increasing importance of lateral fluid flow during crust formation:

$$wt(x,t) = w\exp[-0.003t] \tag{18}$$

and a dependence on porosity is introduced to simulate the Venturi effect:

$$ws(x,t) = -\frac{wt(t)}{\phi(x,t)} \tag{19}$$

Eq. (19) is used in the differential equations for solutes (Eq. (1)). Depending on the chemical and hydrological parameters used, this expression may lead to unrealistically high fluid flow rates when the porosity is strongly diminished (around 0.1) and the crust is nearly completely formed. To avoid this, the coefficient in the exponential term of Eq. (18) was adjusted in order for the peak fluid flow in the crust never to be greater than the initial fluid flow rate through the sedimentary column.

Bioirrigation, the pumping activity of benthic mega- and macrofauna, is described as a nonlocal mixing, in which pore water is exchanged with bottom water over a relatively long vertical distance in the surface sediment by benthic infauna (Emerson et al., 1984). Nonlocal mixing is expressed by a source/sink term:

$$R_b = BIO(x)(C(0,t) - C(x,t)) \tag{20}$$

where $C(0, t)$ is the bottom water concentration of a given solute and $C(x, t)$ is the concentration of the same solute at depth x and time t. The decrease of bioirrigation with depth in the sediment follows a Gaussian decrease law:

$$BIO(x) = BIO0\exp\left[\frac{x^2}{2xs}\right] \tag{21}$$

where BIO0 is the bioirrigation at 0 depth, in year^{-1}, and xs is the halving depth of bioirrigation, in cm. Thus, BIO0 has dimensions of frequency and is a measure of the intensity of bioirrigation, while xs has dimensions of length and controls the depth of sediment that is affected by bioirrigation.

Bioturbation, the mixing of sediment particles by benthic organisms (Berner, 1980), may partially redistribute shallow authigenic carbonates at cold seeps, provided that complete cementation of the sediment has not taken place. In our model, this process is simulated introducing a depth-dependent bioturbation coefficient, $D_b(x)$ in the differential equations for solids (Eq. (2)):

$$D_b(x) = D_b0\exp\left[\frac{x^2}{2xb}\right] \tag{22}$$

where xb, in cm, is the halving depth of bioturbation.

Assuming that the length of the model sediment column (20 cm) is much smaller than the convection system (Fig. 4), the upwards advection rate in the model column, w, is the sum of the advection rate of deep fluids, a, and the convection rate of seawater, c:

$$w = (c + a) \tag{23}$$

The factor by which deep fluids are diluted by seawater, F_d, is defined as in Henry et al. (1992):

$$F_d = \frac{w}{a} \tag{24}$$

so that in the absence of convection F_d=1. The concentration of unreacted solutes in the mixed fluid, C_{mix}, can be the obtained using a simple two end member mixing ratio:

$$C_{mix} = \frac{aC_{df} + cC_{sw}}{w} \tag{25}$$

where C_{df} is the concentration of solutes in the deep fluids and C_{sw} is the concentration of solutes in seawater. Starting from this fluid chemistry, the

Table A5
Chemical composition of fluids at the lower boundary in model runs which consider convection

F_d[a] (–)	w[b] (cm year^{-1})	a[c] (cm year^{-1})	c[d] (cm year^{-1})	$CH_4(L)$ (mM)	$Ca^{2+}(L)$ (mM)	$HCO_3^-(L)$ (mM)	$CO_2(L)$ (mM)	$H^{14}CO_3^-(L)$ ($\times 10^{-12}$ mM)	$SO_4^{2-}(L)$ (mM)
Section 4.2									
5	10	2	8	32	6.36	16.77	3.11	1.591	6.0
10	10	1	9	32	6.40	17.46	3.39	1.725	6.0
15	10	0.7	9.3	32	6.41	17.69	3.48	1.765	6.0
15	10	0.7	9.3	32	6.75	16.38	3.14	1.786	8.0
15	10	0.7	9.3	32	7.10	15.06	2.79	1.812	10.0
15	10	0.7	9.3	32	7.96	11.81	1.93	1.897	15.0
Section 4.3, scenario 3									
15	10	0.7	9.3	120	6.02	18.19	3.46	1.562	6.0
Section 4.3, scenario 5									
15	10	0.7	9.3	120	5.97	18.32	3.48	1.749	6.0
Section 4.3, scenario 6									
15	10	0.7	9.3	120	6.52	16.08	2.92	1.783	10.0

[a] Factor by which deep fluids are diluted by seawater during convection.
[b] Initial advection rate at the surface.
[c] Advection rate of deep fluids.
[d] Convection rate of seawater.

advancement of the AMO and calcium carbonate precipitation reactions in the upwards portion of the convection cell is investigated with a closed system kinetic model composed of five differential equations (one for each solute) in the form:

$$\frac{\partial(\phi C)}{\partial t} = \sum R(t) \tag{26}$$

where $\sum R(t)$ is the sum of all reactions rates affecting a given solute. The rate equations for AMO and calcium carbonate precipitation are taken from (Eqs. (7), (8) and (16) and kinetic constants are taken from Table A1. This system of five differential equations is solved numerically using the composition of the mixed fluid, C_{mix}, calculated with Eq. (25) as initial conditions, using a $CaCO_3$ concentration of 5 wt.% and a porosity of 0.75. Geochemical investigations at cold seeps are showing that methane-rich rising fluids often contain significant amounts of dissolved sulfate (up to 7 mM; Luff and Wallmann, 2003; Hensen, personal communication), which we interpret as derived from seawater through convective mixing. The persistence of such biogeochemically reactive methane–sulfate mixtures implies that AMO is inhibited during convective mixing for some reason. As Tryon et al. (1999) show, convective cells are spatially and temporally ephemeral features. Thus, little time is available for the slow growing microbial consortia responsible for AMO (Boetius et al., 2000) to colonize sediments where convection is mixing sulfate and methane at depth. To account for only partial reaction of methane and sulfate during convection, the system of Eq. (26) is solved for different reaction times to which correspond different residual sulfate concentrations. In addition, starting from the Ca^{2+}, HCO_3^- and CO_2 concentrations calculated with the closed system kinetic model, the DIC system is then brought into equilibrium with calcium carbonate. The corresponding chemical composition at the lower boundary for the convection runs of Sections 4.2 and 4.3 calculated in this way is shown in Table A5. Finally, to simulate the inhibition of AMO in the lower part of the model column, the rate of AMO used in runs considering convection is defined as:

$$R_{SM}(x,t) = k_{SM}\left(C_{SO_4^{2-}}(x,t)\right) - SO_4^{2-}(L))C_{CH_4}(x,t) \tag{27}$$

References

Aharon, P., Schwarz, H.P., Roberts, H.H., 1997. Radiometric dating of submarine hydrocarbon seeps in the Gulf of Mexico. Geol. Soc. Amer. Bull. 109 (5), 568–579.

Akhmanov, G., Woodside, J., 1998. Mud volcanic samples in the context of the Mediterranean Ridge mud diapiric belt. In: Robertson, A.H.F., Emeis, K.-C., Richter, C., Camerlenghi, A. (Eds.), Proc. O.D.P. Sci. Results, vol. 160. Ocean Drilling Program, College Station, TX, pp. 153–180.

Aloisi, G., Pierre, C., Rouchy, J.-M., Foucher, J.-P., The MEDINAUT scientific party, 2000. Methane-related authigenic carbonates of eastern Mediterranean Sea mud volcanoes and their possible relation to gas-hydrate destabilization. Earth Planet. Sci. Lett. 184, 321–338.

Aloisi, G., Bouloubassi, I., Heijs, S.K., Pancost, R.D., Pierre, C., Sinninghe Damsté, J.S., Gottschal, J.C., Forney, L.J., Rouchy, J.-M., 2002. CH_4-consuming microorganisms and the formation of carbonate crusts at cold seeps. Earth Planet. Sci. Lett. 203, 195–203.

Berner, R.A., 1980. Early Diagenesis—A Theoretical Approach. Princeton Univ. Press.

Boetius, A., Ravenschlag, K., Schubert, C.J., Rickert, D., Widdel, F., Gieske, A., Amann, R., Jørgensen, B.B., Witte, U., Pfannkuche, O., 2000. A marine microbial consortium apparently mediating anaerobic oxidation of methane. Nature 407, 623–626.

Boudreau, B.P., 1996. A method of lines code for carbon and nutrient diagenesis in aquatic sediments. Comput. Geosci. 22 (5), 479–496.

Boudreau, B.P., 1997. Diagenetic Models and their Implementation. Springer-Verlag.

Brown, K.M., 1990. The nature and hydrogeologic significance of mud diapirs and diatremes for accretionary systems. J. Geophys. Res. 95 (B6), 8969–8982.

Burton, E.A., 1993. Controls on marine carbonate cement mineralogy: review and reassessment. Chem. Geol. 105, 163–179.

Carson, B., Suess, E., Strasser, J.C., 1990. Fluid flow and mass flux determinations at vent sites on the Cascadia margin accretionary prism. J. Geophys. Res. 95 (B6), 8891–8897.

Cavagna, S., Clari, P., Martire, L., 1999. The role of bacteria in the formation of cold seep carbonates: geological evidence from Monferrato (Tertiary, NW Italy). Sediment. Geol. 126, 253–270.

Cita, M.B., Ryan, W., Paggi, L., 1981. Prometheus mud breccia. An example of shale diapirism in the Western Mediterranean Ridge. Ann. Géol. Pays Hell. 30, 543–570.

Cita, M.B., Ivanov, M.K., Woodside, J.M. (Eds.), 1996a. Special Issue: The Mediterranean Ridge Diapiric Belt, Mar. Geol., vol. 132, pp. 1–271.

Cita, M.B., Erba, E., Lucchi, R., Pott, M., van der Meer, R., Nieto, L., 1996b. Stratigraphy and sedimentation in the Mediterranean Ridge diapiric belt. Mar. Geol. 132, 131–150.

De Lange, G.L., Brumsack, H.-J., 1998. The occurrence of hydrates in eastern Mediterranean mud dome structures as indicated by pore-water composition. In: Henriet, J.-P., Mienert, J. (Eds.), Gas Hydrates: Relevance to World Margin Stability and Climate Change. Geol. Soc. London Spec. Pub., vol. 137, pp. 167–175.

de Marsily, G., 1981. Hydrogéologie Quantitative. Mason, Colloq. Sci. Terre, Paris.

Emerson, S., Jahnke, R., Heggie, D., 1984. Sediment–water exchange in shallow estuarine sediments. J. Mar. Res. 42, 709–730.

Faugères, J.-C., Gonthier, E., Bobier, C., Griboulard, R., 1997. Tectonic control on sedimentary processes in the southern termination of the Barbados Prism. Mar. Geol. 140, 117–140.

Haese, R.R., Meile, C., Van Cappellen, P., de Lange, G.J., 2003. Carbon geochemistry of cold seeps: methane fluxes and transformation in sediments from Kazan mud volcano, eastern Mediterranean Sea. Earth Planet. Sci. Lett. 212, 361–375.

Haese R.R., Hensen C., Pancost R.D., De Lange, G.J., submitted for publication. Pore water geochemistry of submarine mud volcano sediments (eastern Mediterranean Sea): implications for fluid flow, fluid origin and biogeochemical reactions. Geochim. Cosmochim Acta.

Hales, B., Emerson, S., 1997. Evidence in support of first-order dissolution kinetics of calcite in seawater. Earth Planet. Sci. Lett. 148, 317–327.

Henry, P., Foucher, J.-P., Le Pichon, X., Sibuet, M., Kobayashi, K., Tarits, P., Chamot-Rooke, N., Furuta, T., Schultheiss, P., 1992. Interpretation of temperature measurements from the Kaiko-Nankai cruise: modeling of fluid flow in clam colonies. Earth Planet. Sci. Lett. 109, 355–371.

Henry, P., Le Pichon, X., Lallemant, S., Lance, S., Martin, J.B., Foucher, J.-P., Fiala-Médioni, A., Rostek, F., Guilhaumou, N., Pranal, V., Castrec, M., 1996. Fluid flow in and around a mud volcano field seaward of the Barbados accretionary wedge: results from Manon cruise. J. Geophys. Res. 101 (B9), 20297–20323.

Henry, P., Lallemant, S., Nakamura, K.-I., Tsunogai, U., Mazzotti, S., Kobayashi, K., 2002. Surface expression of fluid venting at the toe of the Nankai wedge and implications for flow paths. Mar. Geol. 187, 119–143.

Hinrichs, K.-U., Hayes, J.M., Sylva, S.P., Brewer, P.G., DeLong, E.F., 1999. Methane-consuming archaeabacteria in marine sediments. Nature 398, 802–805.

Hovland, M., Talbot, M.R., Quale, H., Olaussen, S., Aasberg, L., 1987. Methane-related carbonate cements in pockmarks of the North Sea. J. Sediment. Petrol. 57 (5), 881–892.

Kastner, M., Elderfield, H., Martin, J., 1991. Fluids in convergent margins: what do we know about their composition, origin, role in diagenesis and importance for oceanic chemical fluxes. Philos. Trans. R. Soc. Lond., A 335, 243–259.

Kopf, A., Clennel, B., Camerlenghi, A., 1998. Variations in sediment physical properties and permeability of mud-volcano deposits from Napoli dome and adjacent mud volcanoes. In: Robertson, A.H.F., Emeis, K.-C., Richter, C., Camerlenghi, A. (Eds.), Proc. O.D.P. Sci. Results, vol. 160. Ocean Drilling Program, College Station, TX, pp. 625–643.

Kutschera, W., 2000. Accelerator mass spectrometry at VERA. Proceedings of EPAC 2000, Vienna, Austria.

Lalou, C., Fontugne, M., Lallemand, S.E., Lauriat-Rage, A., 1992. *Calyptogena*-cemented rocks and concretions from the eastern part of Nankai accretionary prism: age and geochemistry of Uranium. Earth Planet. Sci. Lett. 109, 419–429.

Le Pichon, X., the Kaiko-Nankai Scientific Crew, 1991. Water budgets in accretionary wedges: a comparison. Philos. Trans. R. Soc. Lond., A 335, 315–330.

Linke, P., Suess, E., Torres, M., Martens, V., Rugh, W.D., Ziebis, W., Kulm, L.D., 1994. In situ measurements of fluid flow from cold seeps at active continental margins. Deep-Sea Res., Part 1 41 (4), 721–739.

Luff, R., Wallmann, K., 2003. Fluid flow, methane fluxes, carbonate precipitation and biogeochemical turnover in gas hydrate-bearing sediment at Hydrate Ridge, Cascadia Margin: numerical modeling and mass balances. Geochim. Cosmochim. Acta 67 (18), 3403–3421.

Luff, R., Wallmann, K., Grandel, S., Schlüter, M., 2000. Numerical modelling of benthic processes in the deep Arabian Sea. Deep-Sea Res., Part 2 47 (14), 3039–3072.

Luff, R., Wallmann, K., Aloisi, G., 2004. Physical and biogeochemical constraints on carbonate crust formation at cold vent sites: significance for fluid and methane budgets and chemosynthetic biological communities. Earth Planet. Sci. Lett. 221, 337–353.

Macdonald, I., Sager, W.W., Peccini, M.B., 2003. Gas hydrate and chemosynthetic biota in mounded bathymetry at mid-slope hydrocarbon seeps: Northern Gulf of Mexico. Mar. Geol. 198 (1–2), 133–158.

Matsumoto, R., 1990. Vuggy carbonate crust formed by hydrocarbon seepage on the continental shelf of Baffin Island, northeast Canada. Geochem. J. 24, 143–158.

MEDINAUT and MEDINETH Shipboard Scientific Parties, 2000. Linking Mediterranean brine pools and mud volcanism. EOS 81 (625), 631–633.

Mills, H.J., Hodges, C., Wilson, K., MacDonald, I.R., Sobecky, P.A., 2003. Microbial diversity in sediments associated with surface-breaching gas hydrate mounds in the Gulf of Mexico. FEMS Microbiol. Ecol. 46 (1), 39–52.

O'Hara, S.C.M., Dando, P.R., Schuster, U., Bennis, A., Boyle, J.D., Chui, F.T.W., Hatherell, T.V.J., Niven, S.J., Taylor, L.J., 1995. Gas seeps induced interstitial water circulation: observations and environmental implications. Cont. Shelf Res. 15 (8), 931–948.

Paull, C.K., Martens, C.S., Chanton, J.P., Neumann, A.C., Coston, J., Jull, A.J.T., Toolin, L.T., 1989. Old carbon in living organisms and young $CaCO_3$ cements from abyssal brine seeps. Nature 342, 166–168.

Paull, C., Chanton, J.P., Neumann, A.C., Coston, J.A., Martens, C.S., 1992. Indicators of methane-derived carbonates and chemosynthetic organic carbona deposits: examples from the Florida escarpment. Palaios 7, 361–375.

Peckmann, J., Reimer, A., Luth, U., Luth, C., Hansen, B.T., Heinicke, C., Hoefs, J., Reitner, J., 2001. Methane-derived carbonates and authigenic pyrite from the northwestern Black Sea. Mar. Geol. 177, 129–150.

Pierre, C., 1999. The oxygen and carbon isotope distributions in the Mediterranean water masses. Mar. Geol. 153, 41–55.

Ritger, S., Carson, B., Suess, E., 1987. Methane-derived authigenic carbonates formed by subduction-induced pore-water expulsion along the Oregon/Washington margin. Geol. Soc. Amer. Bull. 98, 147–156.

Sakai, H., Gamo, T., Ogawa, Y., Boulègue, J., 1992. Stable isotopic ratios and origins of the carbonates associated with cold seepage at the eastern Nankai Trough. Earth Planet. Sci. Lett. 109, 391–404.

Sammonds, P.R., Meredith, P.G., Main, I.G., 1992. Role of pore fluids in the generation of seismic precursors to shear fracture. Nature 359, 228–230.

Stuiver, M., Polach, H.A., 1977. Discussion on reporting of ^{14}C data. Radiocarbon 29, 24–44.

Suess, E., Bohrmann, G., von Huene, R., Linke, P., Wallmann, K., Lammers, S., Sahling, H., 1998. Fluid venting in the eastern Aleutian subduction zone. J. Geophys. Res. 103 (B2), 2597–2614.

Suess, E., Torres, M., Bohrmann, G., Collier, R.W., Greinert, J., Linke, P., Rheder, G., Trehu, A., Wallmann, K., Winkler, G., Zuleger, E., 1999. Gas hydrate destabilisation: enhanced dewatering, benthic material turnover and large methane plumes at the Cascadia convergent margin. Earth Planet. Sci. Lett. 170, 1–15.

Teichert, B.M.A., Eisenhauer, A., Haase-Schramm, A., Bock, B., Linke, P., 2003. U/Th systematics and ages of authigenic carbonates from hydrate ridge, cascadia convergent margin: recorders of fluid composition and sea level changes. Geochim. Cosmochim. Acta 67 (20), 3845–3857.

Tryon, M.D., Brown, K.M., 2001. Complex flow patterns through Hydrate Ridge and their impact on seep biota. Geophys. Res. Lett. 28 (14), 2863–2867.

Tryon, M.D., Brown, K.M., Torres, M.E., Tréhu, A.M., McManus, J., Collier, R.W., 1999. Measurements of transience and downward fluid flow near episodic methane gas vents, Hydrate Ridge, Cascadia. Geology 27 (12), 1075–1078.

Tryon, M.D., Brown, K.M., Torres, M.E., 2002. Fluid and chemical flux in and out of sediments hosting methane hydrate deposits on Hydrate Ridge, OR: II. Observations and long-term record reveal insights into dynamic driving mechanisms. Earth Planet. Sci. Lett. 201, 541–557.

Van Cappellen, P., Wang, Y., 1996. Cycling of iron and manganese in surface sediments: a general theory for the coupled transport and reaction of carbon, oxygen, nitrogen, sulfur, iron, and manganese. Am. J. Sci. 296, 197–243.

Van Dover, C.L., Aharon, P., Bernhard, J.M., Caylor, E., Doerries, M., Flickinger, W., Gilhooly, W., Goffredi, S.K., Knick, K.E., Macko, S.A., Rapoport, S., Raulfs, E.C., Ruppel, C., Salerno, J.L., Seitz, R.D., Sen Gupta, B.K., Shank, T., Turnipseed, M., Vrijenhoek, R., 2003. Blake Ridge methane seeps: characterization of a soft-sediment, chemosynthetically based ecosystem. Deep-Sea Res., Part 1, Oceanogr. Res. Pap. 50 (2), 281–300.

Wallmann, K., Linke, P., Suess, E., Bohrmann, G., Sahling, H., Schlüter, M., Dählmann, A., Lammers, S., Greinert, J., von Mirbach, N., 1997. Quantifying fluid flow, solute mixing, and biogeochemical turnover at cold vents of the eastern

Aleutian subduction zone. Geochim. Cosmochim. Acta 61 (24), 5209–5219.

Woodside, J.M., Ivanov, M.K., Limonov, A.F., 1998. Shallow gas and gas hydrates in the Anaximander Mountains region, eastern Mediterranean Sea. In: Henriet, J.-P., Meinert, J. (Eds.), Gas Hydrates: Relevance to World Margin Stability and Climate Change, Special Publications, vol. 137. Geological Society, London, pp. 177–193.

Zatsepina, O.Y., Buffet, B.A., 1997. Phase equilibrium of gas hydrate: implications for the formation of hydrate in the deep-sea floor. Geophys. Res. Lett. 24 (13), 1567–1570.